

Comparison of Selected Model Order Reduction methods

Studienarbeit (T3_3101)

im Rahmen der Prüfung zum
Bachelor of Science (B.Sc.)

des Studienganges Angewandte Informatik
an der Dualen Hochschule Baden-Württemberg Karlsruhe

von

Florian Braun

Januar 2018

-Sperrvermerk-

Abgabedatum:	22. Mai 2023
Bearbeitungszeitraum:	14.10.2022 - 22.05.2023
Matrikelnummer, Kurs:	7433149, TINF20B1
Gutachter der Dualen Hochschule:	Lutz Gröll

Eidesstattliche Erklärung

Ich versichere hiermit, dass ich meine Studienarbeit (T3_3101) mit dem Thema:

Comparison of Selected Model Order Reduction methods

gemäß § 5 der "Studien- und Prüfungsordnung DHBW Technik" vom 29. September 2017 selbstständig verfasst und keine anderen als die angegebenen Quellen und Hilfsmittel benutzt habe. Die Arbeit wurde bisher keiner anderen Prüfungsbehörde vorgelegt und auch nicht veröffentlicht.

Ich versichere zudem, dass die eingereichte elektronische Fassung mit der gedruckten Fassung übereinstimmt.

Karlsruhe, den May 20, 2023

Nachname, Vorname

Abstract

This paper presents and compares four different model order reduction methods. These are proper orthogonal decomposition, balanced truncation, modal truncation, and Hankel norm approximation. These methods are applied to the 1D heat equation. The heat equation is modified so that a heating process can be represented. This equation is discretized using the finite element method to obtain a state space representation of the system. The model order reduction methods are compared with respect to the L_2 - and H_∞ Fehler and the runtime.

Contents

List of abbreviations	V
List of Figures	VI
1. Introduction	1
1.1. Problem statement	1
1.2. Outline	1
2. Fundamentals	1
2.1. Heat Equation	2
2.2. Finite Element Method	3
2.3. Singular Value Decomposition	6
2.4. Fundamentals of Control Theory	10
3. Model Order Reduction	12
3.1. Introduction	12
3.2. Proper Orthogonal Decomposition	13
3.3. Balanced Truncation	18
3.4. Modal truncation	21
3.5. Hankel Norm Approximation	24
3.6. Modal Truncation is Equal to Balanced Truncation	27
4. Implementation	28
4.1. Class main	29
4.2. Class solution	29
4.3. Class parameters	30
4.4. Class container	30
4.5. Class createBALRED, createMODTRUNC and createHNA	31
4.6. Class containerFEM	31
4.7. Class createPOD	33
4.8. Measurements	35
5. Comparison of MOR Methods	35
5.1. Time Domain Error	36
5.2. Frequency Domain Error	43
5.3. Processing Time	46
6. Conclusion and Outlook	49

Bibliography	VII
A. Appendix	I
A.1. Deriving matrices for FEM using piecewise linear functions	I
A.2. Proof that matrix M is invertible	III
A.3. Equivalence of picewise linear polynomials and linear interpolation	V

List of abbreviations

BT	Balanced Truncation
DCNF	Diagonal Canonical Form
DE	Differential Equation
DFT	Discrete Fourier Transform
FEM	Finite Element Method
FT	Fourier Transform
FFT	Fast Fourier Transform
HNA	Hankel Norm Approximation
HSVD	Hankel Singular Decomposition
IDFT	Inverse Discrete Fourier Transform
IFFT	Inverse Fast Fourier Transform
LS	Least Squares
LTI	Linear Time Invariant
MOR	Model Order Reduction
MT	Modal Truncation
ODE	Ordinary Differential Equation
PDE	Partial Differential Equation
POD	Proper Orthogonal Decomposition
ROM	Reduced Order Model
SVD	Singular Value Decomposition

List of Figures

2.1. Variance and cumulative variance captured by each column vectors of U and V	9
3.1. Variance of Modes	15
3.2. Leading High Variance Modes	16
3.3. Modes 30 to 35	16
3.4. FEM solution and POD approximation for heat equation	17
3.5. FEM solution and BT approximation for heat equation	21
3.6. FEM solution and MT approximation for heat equation	24
4.1. Class diagram main	29
4.2. Flow chart of main class	29
4.3. Class diagram of MOR and FEM implementation	31
4.4. Flow chart for FEM class	32
5.1. L_2 Error Proper Orthogonal Decomposition $x(0, x) = 1$	37
5.2. Variance of POD Modes	37
5.3. L_2 POD error $n = 100$, $x(0, x) = 1$	38
5.4. L_2 Error Proper Orthogonal Decomposition $x(0, x) = \sin(\frac{2\pi}{L}x)$	39
5.5. L_2 POD error	39
5.6. L_2 Error Balanced Truncation	40
5.7. L_2 Error Balanced Truncation	41
5.8. L_2 Error Hankel Norm Approximation	42
5.9. Box Plot of L_2 Error	42
5.10. H_∞ error of POD	44
5.11. H_∞ error of Balanced Truncation and Modal Truncation	44
5.12. H_∞ error of Hankel Norm Approximation	45
5.13. Box Plot of H_∞ error	46
5.14. Processing time POD	47
5.15. Processing time MT	48
5.16. Processing time BT	48
5.17. Processing time HNA	49

1. Introduction

With the development of semiconductor-based computers, humanity has access to the most powerful computing machines ever created. Still, those cutting-edge technologies often need to provide more computational power to solve problems in maths, physics, or engineering. Often those problems appear as partial differential equations. Discretizing PDEs into systems of ordinary differential equations allows the generation of approximate solutions. This resulting system of ODEs is often still too large to use for computations directly. Methods to reduce the size of those systems are called model order reduction methods.

1.1. Problem statement

Various model reduction methods can be chosen based on the problem and its setting. Each of them approximates the original system in some optimal manner. This paper aims to compare the properties of a defined set of model order reduction methods. The compared properties are the error of the reduced order models and the time it takes to compute them. The system that gets reduced describes the heat transfer in a piece of wire that can be heated or cooled arbitrarily.

1.2. Outline

The fundamentals are covered first. It begins with the basics of the heat equation and how the already mentioned heating or cooling works, respectively. Also, some naive method to obtain an approximate solution is covered. However, the next part of that chapter will discuss the finite element method since this technique is more powerful than the previously stated method. After that, the singular value decomposition is covered since it sees much usage in the model order reduction methods. Since most methods come from control theory, the subsequent section covers some basic control theory. Chapter three is about the workings of the model order reduction methods. It begins with the proper orthogonal decomposition. Balanced truncation, modal truncation, and Hankel norm approximation follow. Last but not least, it gets demonstrated that modal truncation equals balanced truncation for this system. In chapter four, the implementation of those methods and the implementation of the finite element solver is discussed. After that, the conduction of numerical experiments takes place. Here the time domain error, frequency domain error, and the time it takes to compute the reduced order models are measured and compared.

2. Fundamentals

This chapter covers the fundamentals necessary for understanding the model order reduction methods. First of all, a system to apply those methods is needed. Here the 1D heat equation was chosen since it is fairly easy to solve and to understand the results. After that, the method of finite elements is introduced. This method discretizes the 1D heat equation into a solvable system of ODEs since it can handle boundary conditions and initial values. One of the most important fundamentals of this paper is the singular value decomposition since it takes heavy use in the model order reduction methods covered. The last Section of this chapter will cover some control theory fundamentals. Those are needed since three model order reduction methods appear in a control theory context. Hence some explanation of the terminology is needed.

2.1. Heat Equation

The following partial differential equation (PDE) describes the conduction of heat within a medium

$$\frac{\partial u}{\partial t} = \alpha \nabla^2 u. \quad (2.1)$$

Here u is a function of space and time, and α is a positive constant. For this paper u will be defined in terms of one spatial dimension [1]

$$u := u(x, t) \quad (2.2)$$

$$\frac{\partial u}{\partial t} = \alpha \frac{\partial^2 u}{\partial x^2} \quad (2.3)$$

$$x \in \chi \subset \mathbb{R} \quad t \in \tau \subset \mathbb{R} \quad (2.4)$$

$$x_0 \leq x \leq x_n \quad t_0 \leq t \leq t_n. \quad (2.5)$$

In order to model the conduction of heat within a medium but also a heating process, a new function $h : \chi \times \tau \rightarrow \mathbb{R}$ is introduced:

$$\frac{\partial u}{\partial t} = \alpha \frac{\partial^2 u}{\partial x^2} + h(x, t). \quad (2.6)$$

For this paper, the assumption is made that the initial condition is known

$$f : \chi \rightarrow \mathbb{R} \quad (2.7)$$

$$u(x, t_0) = f(x). \quad (2.8)$$

Applying the Fourier transform (FT) w.r.t x to (2.6) yields the inhomogeneous ordinary differential equation (ODE)

$$\hat{u} = \mathfrak{F}(u) \quad \hat{h} = \mathfrak{F}(h) \quad (2.9)$$

$$\frac{d}{dt}\hat{u} = -\alpha\omega^2\hat{u} + \hat{h}. \quad (2.10)$$

A solution to (2.10) is given by

$$\hat{u} = \hat{u}_0 + \hat{u}_p. \quad (2.11)$$

Where \hat{u}_0 is the homogeneous solution and \hat{u}_p is the particular integral. In order to solve this ODE, the particular integral \hat{h} has to be known [2]. The choice of h is, except for some restrictions, arbitrary. Therefore an approximate solution to 2.10 \hat{u}_a is obtained by the forward Euler scheme

$$\frac{d}{dt}\hat{u} \approx \frac{\Delta\hat{u}}{\Delta t} \quad (2.12)$$

$$\hat{u}_{t+1} = \hat{u}_t + \Delta t(-\alpha\omega^2\hat{u} + \hat{h}) \quad (2.13)$$

$$\hat{u}_a = [\hat{u}_{t_0} \quad \cdots \quad \hat{u}_{t_n}]. \quad (2.14)$$

The Euler scheme is applicable if an initial condition \hat{u}_0 is known. This initial condition is obtained by applying the discrete Fourier transform (DFT) to an initial temperature distribution along x [3]

$$\hat{u}_0 = \mathfrak{F}\{f(x)\}. \quad (2.15)$$

The forward Euler scheme is used because it is easy to implement. Applying the inverse discrete Fourier transform (IDFT) to \hat{u}_a , an approximate solution to (2.6) can be obtained. Using fast Fourier transform (FFT) and inverse fast Fourier transform (IFFT) instead of the DFT, and IDFT reduces the processing time. This method for solving the heat equation raises the problem that it cannot handle boundary conditions. Using the finite element method, the heat equation is solvable as an initial boundary value problem (IBVP).

2.2. Finite Element Method

The finite element method (FEM) is a method to approximate solutions for differential equations (DE) within a certain domain Ω , by discretizing the spatial domain. Assume that a DE

is given by

$$m, n \in \mathbb{N} \quad \zeta \in \Omega \subset \mathbb{R} \quad m \geq 1 \quad (2.16)$$

$$\frac{\partial^m y}{\partial \zeta^m} - g(y) = r(\zeta, t). \quad (2.17)$$

Assuming that g is a linear function that can also contain partial derivatives of y w.r.t. time, y takes the value 0 at the boundary Γ and $y(\zeta, 0) = f(\zeta)$. An approximate solution to y is given by μ , which is expressed as a sum of basis functions contained in the set ϕ :

$$\mu(\zeta, t) = \sum_{j=1}^N c_j(t) \phi_j(\zeta). \quad (2.18)$$

The definition of the residual is as follows

$$\mathbf{r} = \frac{\partial^m \mu}{\partial \zeta^m} - g(\mu) - r(\zeta, t). \quad (2.19)$$

Furthermore, the residual is required to be orthogonal to all basis functions

$$\langle \mathbf{r}, \phi_k \rangle = 0 \quad \forall \phi_k \in \phi. \quad (2.20)$$

Since the functions in ϕ are known, it is only required to find the coefficients $c_j(t)$ in (2.18). To find those coefficients (2.20) needs to be expressed as follows

$$\int_{\Omega} \frac{\partial^m \mu}{\partial \zeta^m} \phi_k d\zeta - \int_{\Omega} g(\mu) \phi_k d\zeta = \int_{\Omega} r(\zeta, t) \phi_k d\zeta \quad \forall \phi_k \in \phi. \quad (2.21)$$

If μ is substituted with (2.18) the following is obtained

$$\sum_{j=1}^N \left(\left(\int_{\Omega} \frac{\partial^m \phi_j}{\partial \zeta^m} \phi_k d\zeta \right) c_j(t) - g \left(\left(\int_{\Omega} \phi_k \phi_j d\zeta \right) c_j(t) \right) \right) = \int_{\Omega} r(\zeta, t) \phi_k d\zeta \quad \forall \phi_k \in \phi. \quad (2.22)$$

It is also necessary to apply the divergence theorem to the first integral term considering that y at Γ is 0. Since ζ is one dimensional, the divergence theorem becomes integration by parts

$$\int_{\Omega} \frac{\partial^m \phi_j}{\partial \zeta^m} \phi_k d\zeta = - \int_{\Omega} \frac{\partial^{m-1} \phi_j}{\partial \zeta^{m-1}} \frac{\partial \phi_k}{\partial \zeta} d\zeta \quad \forall \phi_k \in \phi. \quad (2.23)$$

Combining (2.22) and (2.23) yields

$$- \sum_{j=1}^N \left(\left(\int_{\Omega} \frac{\partial^{m-1} \phi_j}{\partial \zeta^{m-1}} \frac{\partial \phi_k}{\partial \zeta} d\zeta \right) c_j(t) + g \left(\left(\int_{\Omega} \phi_k \phi_j d\zeta \right) c_j(t) \right) \right) = \int_{\Omega} r(\zeta, t) \phi_k d\zeta \quad \forall \phi_k \in \phi. \quad (2.24)$$

This formulation leads to a system of ODEs or linear equations that can be solved numerically.

2.2.1. Solving the Heat Equation using FEM

This formulation of FEM applies to (2.6)

$$\Omega = \chi \quad \Gamma = \{x_0, x_n\} \quad (2.25)$$

$$y(\zeta, t) = -u(x, t) \quad g(u) = -\frac{1}{\alpha} \frac{\partial u}{\partial t} \quad (2.26)$$

$$m = 2 \quad r(\zeta, t) = \frac{1}{\alpha} h(x, t) \quad (2.27)$$

$$u(x, 0) = f(x) \quad u(x_0, t) = 0 \quad u(x_n, t) = 0. \quad (2.28)$$

The set of basis functions is defined as a set of piecewise linear functions with constant step size Δx [4]

$$\phi_j(x) = \begin{cases} (x - x_{j-1})/\Delta x, & x_{j-1} \leq x < x_j \\ (x_{j+1} - x)/\Delta x, & x_j \leq x < x_{j+1} \\ 0, & \text{otherwise} \end{cases} \quad (2.29)$$

The step size Δx is defined by $\Delta x = \frac{x_n - x_0}{n-1}$. This results in the following system of ODEs

$$\sum_{j=1}^N \left(\int_{\chi} \phi_j \phi_k dx \right) \frac{dc_j}{dt} = \alpha \sum_{j=1}^N \left(- \int_{\chi} \frac{d\phi_j}{dx} \frac{d\phi_j}{dx} dx \right) c_j(t) + \int_{\chi} h(x, t) \phi_k dx \quad \forall \phi_k \in \phi. \quad (2.30)$$

Since $\phi_k \phi_j \neq 0$ for $k = j, k = j \pm 1$ (2.30) can be expressed as

$$q_1 \dot{c}_{j-1} + q_2 \dot{c}_j + q_1 \dot{c}_{j+1} = p_1 c_{j-1} + p_2 c_j + p_1 c_{j+1} + H(x, t). \quad (2.31)$$

where p and q are some constants derived later. For $j = 1$ and $j = n$ some new coefficients c_0, c_{n+1} are introduced. They are set to zero $c_0 = c_{n+1} = 0$ to force the boundary condition. It follows that $h(x, t)$ and $c_j(0)$ have to satisfy the boundary condition too.

Using matrix notation, this becomes

$$M^{N \times N}, K^{N \times N} \quad (2.32)$$

$$M \dot{c} = Kc + d. \quad (2.33)$$

The matrices M and K can be easily computed (Appendix A.1)

$$m_{ij} = \begin{cases} \frac{2\Delta x}{3}, & k = j \\ \frac{\Delta x}{6}, & |k - j| = 1 \\ 0, & \text{otherwise} \end{cases} \quad k_{ij} = \begin{cases} \frac{-2\alpha}{\Delta x}, & k = j \\ \frac{\alpha}{\Delta x}, & |k - j| = 1 \\ 0, & \text{otherwise} \end{cases} \quad (2.34)$$

Furthermore, to solve this system of ODEs numerically, an initial condition c_0 has to be known [3]. The least squares (LS) approach is used to obtain the initial condition [5]

$$\sum_{j=1}^N \langle \phi_j, \phi_k \rangle c_j(0) = \langle f, \phi_k \rangle \quad \forall \phi_k \in \phi \quad (2.35)$$

$$M c_0 = F \quad (2.36)$$

$$c_0 = M^{-1} F. \quad (2.37)$$

However, since the basis functions are piecewise linear, the coefficients are $c_0 = [f(0), f(\Delta x), \dots, f(n)]^T$ [6]. It is necessary to approximate d for each point in time using numerical integration schemes. By assuming that the following decomposition holds

$$h(x, t) = \sum_{i=1}^N \phi_i(x) v(t). \quad (2.38)$$

the vector d in (2.33) can be expressed as $M v(t)$. Observe that by multiplying (2.33) with M^{-1} (A.2) yields a system of ODEs

$$\dot{c} = M^{-1} K c + M^{-1} M v. \quad (2.39)$$

This system of ODEs can be solved using an Euler scheme

$$c_{t+1} = \Delta t (M^{-1} K c_t + I v) + c_t. \quad (2.40)$$

The function $u(x, t)$ can be approximated via the computed coefficients and (2.18) However this is equivalent to linear interpolation between c_n and c_{n+1} (Appendix A.3).

2.3. Singular Value Decomposition

The Singular Value Decomposition (SVD) is a matrix factorization with guaranteed existence. It can be used to obtain low-rank approximations of a matrix or pseudo inverses for an ill-posed linear system of equations. It is also related to FT by providing a data-specific set of orthogonal bases instead of a generic set of sines and cosines. For this paper, the SVD will be used for generating low-rank approximations of matrices [7].

2.3.1. Properties

A matrix $X \in \mathbb{R}^{n \times m}$ can be decomposed in the following way

$$X = U \Sigma V^T. \quad (2.41)$$

Here $U \in \mathbb{R}^{n \times n}$ and $V \in \mathbb{R}^{m \times m}$ are unitary matrices and $\Sigma \in \mathbb{R}^{n \times m}$ is a real valued ordered diagonal matrix. The columns of U provide a set of orthonormal basis vectors for the column space of X , and V contains orthonormal basis vectors for the row space of X . The matrix Σ assigns a magnitude ('importance') to the product of U and V^T [8]. Since U and V are unitary they have the following property [9]

$$U^T U = U U^T = I \quad (2.42)$$

$$V^T V = V V^T = I. \quad (2.43)$$

In case $n \geq m$, the so-called economy SVD can be used to factorize the matrix X

$$X = \begin{bmatrix} \hat{U} & \hat{U}^\perp \end{bmatrix} \begin{bmatrix} \hat{\Sigma} \\ 0 \end{bmatrix} V^T = \hat{U} \hat{\Sigma} V^T. \quad (2.44)$$

The economy SVD omits rows only containing zeros in Σ and the according columns of U . Therefore the dimensionality of \hat{U} and $\hat{\Sigma}$ is less or equal to the dimensionality of U and Σ [7].

2.3.2. Hierarchy of correlations

As already stated, the matrix Σ assigns a magnitude to UV^T . This magnitude is the square of the variance of the bases in U and V capture. Assume that $X^T X$ and $X X^T$ denote correlation matrices [7]. A correlation matrix is a matrix that stores correlation coefficients between multiple measurements. If X has the following properties $X^T X$ and $X X^T$ are correlation matrices.

1.) The column vectors of X have to be zero mean

$$X = \begin{bmatrix} x_1 & \cdots & x_m \end{bmatrix} \quad (2.45)$$

$$\frac{1}{n} \sum_{i=1}^n x_{ij} = \mu_i = 0, \quad 1 \leq i \leq m. \quad (2.46)$$

2.) The column vectors of X have to be normalized

$$\sqrt{\sum_{i=1}^n x_{ij}^2} = \bar{x}_i = 1, \quad 1 \leq i \leq m. \quad (2.47)$$

The correlation coefficient between two column vectors of X is calculated as follows [10]

$$\text{corr}(x_i, x_{i'}) = \frac{(\sum_{j=1}^n x_{ij} - \bar{x}_i)(\sum_{j=1}^n x_{i'j} - \bar{x}_{i'})}{(\sum_{j=1}^n (x_{ij} - \bar{x}_i)^2)^{\frac{1}{2}} (\sum_{j=1}^n (x_{i'j} - \bar{x}_{i'})^2)^{\frac{1}{2}}}. \quad (2.48)$$

Since all column vectors have zero means and are normalized, this becomes [11]

$$\text{corr}(x_i, x_{i'}) = \text{cov}(x_i, x_{i'}) = x_i^T x_{i'}. \quad (2.49)$$

This resembles the entries of XX^T and $X^T X$. A vector e that maximizes the variance of the projection of x_i onto e with the restriction $\|e\| = 1$ are the eigenvectors of the according correlation matrix. The eigenvalue of e denoted as λ is equivalent to the variance of x_i projected onto e [12].

Since X can be de-constructed using the SVD, XX^T and $X^T X$ are equal to

$$XX^T = U \begin{bmatrix} \hat{\Sigma} \\ 0 \end{bmatrix} V^T V \begin{bmatrix} \hat{\Sigma} & 0 \end{bmatrix} U^T = U \begin{bmatrix} \hat{\Sigma}^2 & 0 \\ 0 & 0 \end{bmatrix} U^T \quad (2.50)$$

$$X^T X = V \begin{bmatrix} \hat{\Sigma} & 0 \end{bmatrix} U^T U \begin{bmatrix} \hat{\Sigma} \\ 0 \end{bmatrix} V^T = V \hat{\Sigma}^2 V^T. \quad (2.51)$$

By multiplying U and V respectively on the right side (2.50) and (2.51) become

$$XX^T U = U \begin{bmatrix} \hat{\Sigma}^2 & 0 \\ 0 & 0 \end{bmatrix} \quad (2.52)$$

$$X^T X V = V \hat{\Sigma}^2. \quad (2.53)$$

This shows that V contains the eigenvectors of the row-wise correlation matrix, and U contains the eigenvectors of the column-wise correlation matrix. The matrix Σ contains the roots of the according eigenvalues and is related to the variance. By ordering U , Σ and V by the entries of Σ in a descending order the first row of U and V contain the most important basis vectors [7].

2.3.3. Low-rank approximation

A useful property of the SVD is that it can be used to find a hierarchy of rank- r approximations for a given matrix X . An matrix \tilde{X} that approximates X is obtained by

$$\tilde{X} = \underset{s.t. \text{rank}(\tilde{X})=r}{\text{argmin}} \|X - \tilde{X}\|_F = \tilde{U} \tilde{\Sigma} \tilde{V}^T \quad (2.54)$$

Here \tilde{U} and \tilde{V} denote matrices obtained taking the first r columns of U and V . The matrix $\tilde{\Sigma}$ is a $r \times r$ sub-block of Σ . This is also known as the Eckard-Young theorem. The variance

captured by \tilde{X} can be calculated in the following way [7]

$$\text{cumvar}_r(\Sigma) = \frac{\sum_{i=1}^r \sigma_i}{\text{trace}(\Sigma)} \quad (2.55)$$

$$\text{var}(\Sigma) = \frac{\text{diag}(\Sigma)}{\text{trace}(\Sigma)}. \quad (2.56)$$

2.3.4. Example low-rank approximation

As an example, suppose there is a matrix X

$$X = \begin{bmatrix} 3 & 1 & 5 & 5 \\ 4 & -4 & 5 & 0 \\ -4 & -2 & -4 & 3 \\ 5 & 1 & 5 & -4 \end{bmatrix}. \quad (2.57)$$

By computing the SVD the matrices U , Σ and V are obtained. Now Σ can be used to calculate the cumulative variance for a rank- r approximation and the variance captured by each basis vector of U and V .

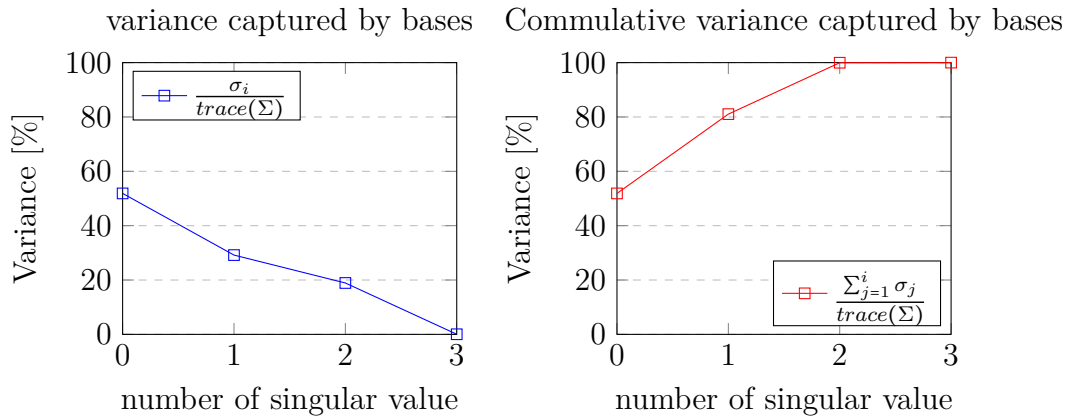


Figure 2.1.: Variance and cumulative variance captured by each column vectors of U and V

In figure 2.1, the commutative variance and the variance of each basis vector are plotted. Here X can be approximated using the first three leading basis vectors. This approximation captures already more than 99% of the variance. The resulting matrix \tilde{X}_3 looks as follows

$$\tilde{X}_3 = \begin{bmatrix} 4.73 & -0.76 & 5.62 \\ 1.31 & -1.37 & 1.62 \\ -5.10 & -0.60 & 2.34 \end{bmatrix}. \quad (2.58)$$

2.4. Fundamentals of Control Theory

There are mainly three different problems in control theory. A system has to be identified before it can be analyzed. A mathematical model has to be found that relates the input of that system to its output. After a model has been found, it is helpful to simulate the system to determine which input results in which output. Simulations have to fit the system and offer the advantage over real experiments in reducing costs and risks attached to them. The last of the three major problems is the control problem. Now that the underlying model is known and the system can be simulated, designing a controller for that system is possible. Here the controller is a system that feeds some input to the controlled system to generate some desired output [13]. For this paper, the second problem is the most important one since the goal of this paper is to compare some methods to make simulations of a system more efficient.

2.4.1. LTI Systems

A linear time-invariant (LTI) system is a kind of system that fulfills the following conditions:

Homogeneity: One of the conditions for a system to be an LTI system, is that the output of a system $y(t)$ relates to the input $u(t)$ and the initial condition x_0 by a linear operator f

$$y(t) = f(u(t), x_0) \quad (2.59)$$

$$cy(t) = f(cu(t), x_0). \quad (2.60)$$

This means that if the input u changes in magnitude by a constant factor of c , the output y also changes by the factor of c .

Superposition: The second requirement is superposition

$$y_1(t) + y_2(t) = f(u_1(t) + u_2(t), x_0). \quad (2.61)$$

The sum of two outputs y_1 and y_2 has to equal the output of the system with the sum of the inputs u_1 and u_2 as input.

Time Invariance: A time-invariant system has the property that if the input u is shifted in time by some constant τ , the resulting output is also shifted in time by the same constant

$$y(t - \tau) = f(u(t - \tau), x_0). \quad (2.62)$$

LTI systems are important because they can be used to approximate non-LTI systems over some region. This is useful since LTI systems are well understood [14].

2.4.2. State Space Representation

An LTI system can be expressed as a system of ODEs that relates the input u to its output y . The vector x denotes the states of a system.

$$\dot{x} = Ax + Bu \quad x(0) = x_0 \quad (2.63)$$

$$y = Cx + Du \quad (2.64)$$

The matrices $A \in \mathbb{R}^{n \times n}$, $B \in \mathbb{R}^{n \times m}$, $C \in \mathbb{R}^{q \times n}$ and $D \in \mathbb{R}^{q \times m}$ are constant matrices [15].

2.4.3. State Space of Discrete-Time Systems

A system can be represented as a discrete system in the following form

$$x_{k+1} = A_d x_k + B_d u_k \quad (2.65)$$

$$y_{k+1} = C_d x_k + D_d u_k \quad (2.66)$$

$$x_k = x_{k\Delta t} . \quad (2.67)$$

The matrices A_d to D_d can be obtained from the continuous system in the following way [16]

$$A_d = e^{A\Delta t}, \quad B_d = \int_0^{\Delta t} e^{A\tau} B d\tau, \quad C_d = C, \quad D_d = D . \quad (2.68)$$

2.4.4. Transfer Function

To understand the transfer function, the impulse response has to be defined first. The impulse response of a system is given by choosing the delta function as input to the system

$$\delta(t) = \begin{cases} \infty, & t = 0 \\ 0 & else \end{cases} \quad g(t) = f(\delta(t)) . \quad (2.69)$$

It has the property that the integral of this function is 1

$$\int_{t=-\infty}^{\infty} \delta(t) dt = 1 . \quad (2.70)$$

If the $g(t)$ is convoluted with a function $v(t)$ the response of the system for $v(t)$ as input is obtained [17]

$$v(t) * g(t) = \int_{\tau=0}^{\infty} v(\tau) g(t - \tau) d\tau = f(v(t)) . \quad (2.71)$$

By using the convolution theorem [18]

$$\mathcal{L}\{g(t)\}\mathcal{L}\{v(t)\} = \mathcal{L}\{g * v\}(t). \quad (2.72)$$

the definition of the transfer function is as follows

$$\mathcal{L}\{f(\delta(t))\}. \quad (2.73)$$

This definition is useful since the response of a system for a given input $u(t)$ can be determined by the result of the multiplication $G(s)U(s)$ [17]. Alternatively, for a system in state space representation, the transfer function is [15]

$$G(s) = C(sI - A)^{-1}B + D. \quad (2.74)$$

2.4.5. Controllability and Observability

For LTI systems in state space representation, it can be determined which states are to what degree controllable and observable. The controllability and observability of gramians can compute this

$$W_c = \lim_{t \rightarrow \infty} \int_0^t e^{A\tau} B B^* e^{A^* \tau} d\tau \quad (2.75)$$

$$W_o = \lim_{t \rightarrow \infty} \int_0^t e^{A^* \tau} C^* C e^{A\tau} d\tau. \quad (2.76)$$

The degree of controllability for a state x can be determined by $x^* W_c x$. If the result of this calculation is large, the system is controllable in the x direction. By swapping W_c with W_o the degree of observability in state x can be computed: $x^* W_o x$. Again if the resulting value is large, the system can be observed well in the state x [19].

3. Model Order Reduction

3.1. Introduction

Model Order Reduction (MOR) is a technique to reduce the computational effort of simulating a system using mathematical models. This reduction in effort is done by using two different approaches. The first uses a numerical approach, and the second utilizes system theory. The first method discussed is called Proper Orthogonal Decomposition. After that, Balanced and Modal truncation will be discussed. The last method discussed will be Hankel-norm approximation [20].

3.2. Proper Orthogonal Decomposition

The proper orthogonal decomposition (POD) is a method for model order reduction. The reduction in computational effort is done by approximating a solution to a PDE using an orthogonal expansion. Decomposing a set of solutions for the PDE using the SVD yields a set of basis functions.

3.2.1. Orthogonal Expansion

A function $f : \mathbb{R} \times \mathbb{R} \rightarrow \mathbb{R}$ can be represented by the series

$$f(x, t) = \sum_{i=1}^{\infty} a_i(t) \phi_i(x). \quad (3.1)$$

Here all $\phi(x)$ are orthogonal basis functions

$$\langle \phi_i, \phi_j \rangle = \begin{cases} 1, & \text{if } i = j \\ 0, & \text{else} \end{cases}. \quad (3.2)$$

By using a finite sum instead of the entire series f can be approximated

$$\tilde{f}(x, t) = \sum_{i=1}^n a_i(t) \phi_i(x). \quad (3.3)$$

Since all ϕ are known, (3.3) has to be solved for the set $\{a_0, \dots, a_n\}$. In case f is known, the solutions contained in this set can be calculated as

$$a_i(t) = \frac{\langle \phi_i, f \rangle}{\langle \phi_i, \phi_i \rangle}. \quad (3.4)$$

[21]

3.2.2. Proper Orthogonal Decomposition for PDEs

Since PDEs are equations in terms of partial derivatives, the notation $\mathfrak{P}(\partial x)u$ is introduced, which denotes a differential operator in terms of the spatial variables x for a function $u(x, t, p)$. The vector p contains some parameters. This notation provides a more abstract way to denote PDEs [22]

$$\frac{\partial u}{\partial t} = \mathfrak{P}(\partial x)u. \quad (3.5)$$

Solving for u is often difficult to impossible. A common method to solve PDEs is called the separation of variables. This separation of variables assumes that the underlying solution

$u(x, t)$ can be expressed by (3.1), where it has to be solved for $a_k, 0 \leq k \leq n$. Since it is not practical to compute an infinite series, u only gets approximated by using (3.3) instead

$$\sum_{i=1}^n \frac{\partial a_i}{\partial t} \phi_i = \sum_{i=1}^n \mathfrak{P}(\partial x) \phi_i a_i. \quad (3.6)$$

By discretizing the spatial dimension along x (3.6) can be expressed using matrix notation

$$\Phi = [\phi_0 \quad \dots \quad \phi_n] \quad (3.7)$$

$$\Phi \frac{d}{dt} a = \mathfrak{P}(\partial x) \Phi a. \quad (3.8)$$

Since the solution u is unknown (3.4) cannot be computed. However, the fact that all ϕ are orthogonal to each other can be used to solve for all a_k . It can be done by computing the inner product of (3.6) with all basis functions

$$\left\langle \sum_{i=1}^n \frac{\partial a_i}{\partial t} \phi_i, \phi_k \right\rangle = \left\langle \sum_{i=1}^n \mathfrak{P}(\partial x) \phi_i a_i, \phi_k \right\rangle, \quad 0 \leq k \leq n. \quad (3.9)$$

This resembles the Galerkin projection. In matrix notation, it can be expressed

$$\Phi^T \Phi \frac{d}{dt} a = \Phi^T \mathfrak{P}(\partial x) \Phi a. \quad (3.10)$$

By considering (3.2), the equation (3.9) can be expressed as a system of ODEs which can be solved

$$\frac{d}{dt} a = \Phi^T \mathfrak{P}(\partial x) \Phi a. \quad (3.11)$$

After the vector of coefficients a been computed for each time step has, the solution can be assembled [23]

$$u(x, t) \approx \Phi(x) a(t). \quad (3.12)$$

3.2.3. Selection of Basis Vectors

As discussed in the previous section, a set of basis vectors can be used to generate approximate solutions to PDEs. However, it was not discussed how those basis vectors are chosen. For POD to work, a so-called snapshot matrix X has to be available. This snapshot matrix stores a set of solutions where x_k is the solution for a PDE at time step $k\Delta t$

$$X = [x_1 \quad \dots \quad x_m]. \quad (3.13)$$

The solutions can be obtained by experimenting on a physical system that is described by the PDE or by simulating the evolution of that PDE. In this paper, the solution is obtained using FEM from section 2.2. SVD is used to decompose the snapshot matrix X . Since the columns of the snapshot matrix contain spatial information at a given point in time and the basis vectors are supposed to encode the spatial information of a solution u , the r most dominant left singular values have to be extracted

$$\tilde{X} = \tilde{U} \tilde{\Sigma} \tilde{V}^T \quad (3.14)$$

$$\Phi = [u_1 \quad \cdots \quad u_r] . \quad (3.15)$$

Here the FEM solution is obtained by discretizing the PDE into a large number(n) of spatial nodes. This results in a high-dimensional system of ODEs. Since Φ contains only r column ($r \ll n$) vectors a reduction in order can be achieved. The number of modes r is determined by the variance that has to be persevered. Figure 3.1 shows the variance each mode stores. Here the first two modes already store almost 97% of the variance.

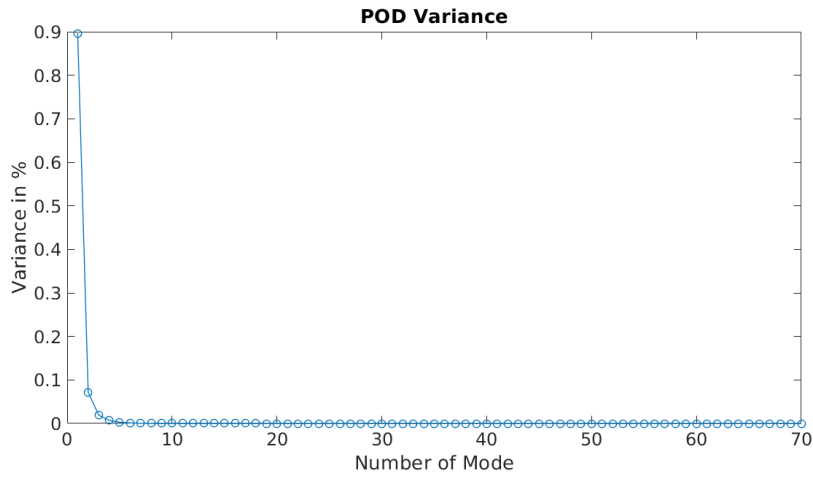


Figure 3.1.: Variance of Modes

These two modes are displayed in figure 3.2.

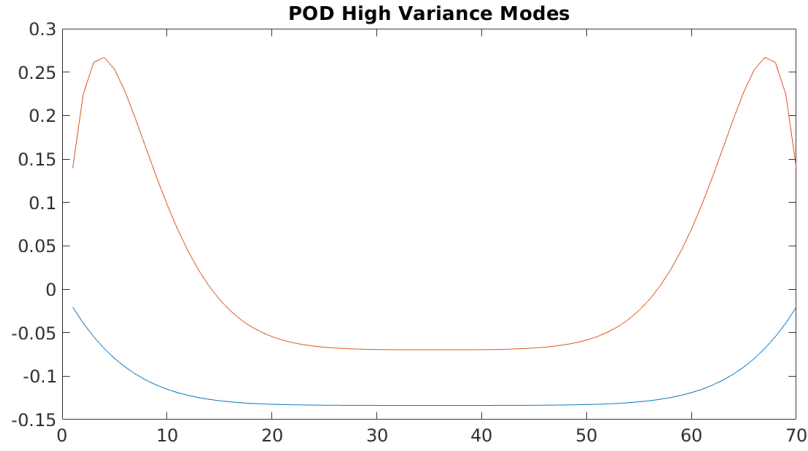


Figure 3.2.: Leading High Variance Modes

Setting the variance too high also includes low variance modes that will introduce some errors. Some low variance modes are displayed in figure 3.3.

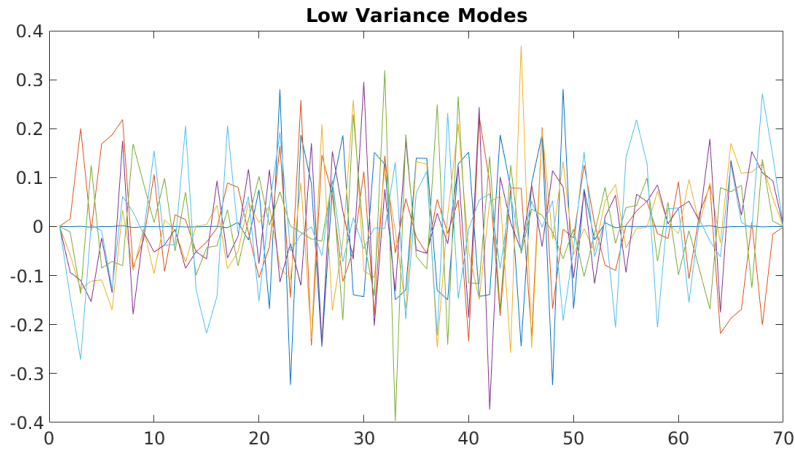


Figure 3.3.: Modes 30 to 35

Figure 3.1 shows that modes 30 to 35 almost have zero contribution to the snapshot matrix. Therefore including them will introduce noise to the approximation and will increase computations. However, the benefits of this reduced order model are only relevant after the PDE has been solved once using a high dimensional system of ODEs [23].

3.2.4. POD for Heat Equation

In order to apply pod to the heat equation, a snapshot matrix X has to be generated. The snapshot matrix is generated by the FEM solver described in section 2.2. After that, X gets

decomposed using the SVD. The modes contained in Φ are obtained by truncating the left singular vectors of X according to (3.15). Substituting \mathfrak{P} in (3.12) with heat equation 2.6 results in the following

$$\Phi \frac{\partial a}{\partial t} = \alpha \frac{\partial^2 \Phi}{\partial x^2} a + h \quad (3.16)$$

$$\frac{\partial a}{\partial t} = \alpha \Phi^T \frac{\partial^2 \Phi}{\partial x^2} a + \Phi^T h. \quad (3.17)$$

This system of ODEs can now be solved using Euler scheme. Note that Φ contains numeric values. Therefore derivatives are unstable, especially at the first and last entries of the column vectors of Φ . To reduce this problem, the method used to compute the second derivative of Φ is the so-called spectral derivative. The discrete spectral derivative works by computing the FFT of a vector. That vector is multiplied by $(ik)^d$, d is the order of the derivative, and k are the discrete wave numbers. After that step, the IFFT is applied to obtain the derivative of the original vector [24]

$$f \in \mathbb{C}^n, \quad k = \left[\frac{n}{2} \quad \dots \quad \frac{n}{2} \right]^T \quad (3.18)$$

$$\frac{df}{dx} = \mathfrak{F}^{-1} \left\{ i \frac{2\pi k}{n} \mathfrak{F}\{f\} \right\} \quad (3.19)$$

$$\frac{d^2 f}{dx^2} = \mathfrak{F}^{-1} \left\{ -\frac{2\pi k}{n} \mathfrak{F}\{f\} \right\}. \quad (3.20)$$

Figure 3.4 shows a solution to heat equation using FEM and an approximation using POD with $u(x, t) = 0, x_0 = 10000^{70 \times 1}, n = 70$, variance = 90%. The x-axis displays time in seconds, and the y-axis is the object's length. It is visible that there are some differences, especially near the boundaries. However, chapter 5 covers a more detailed analysis of the error.

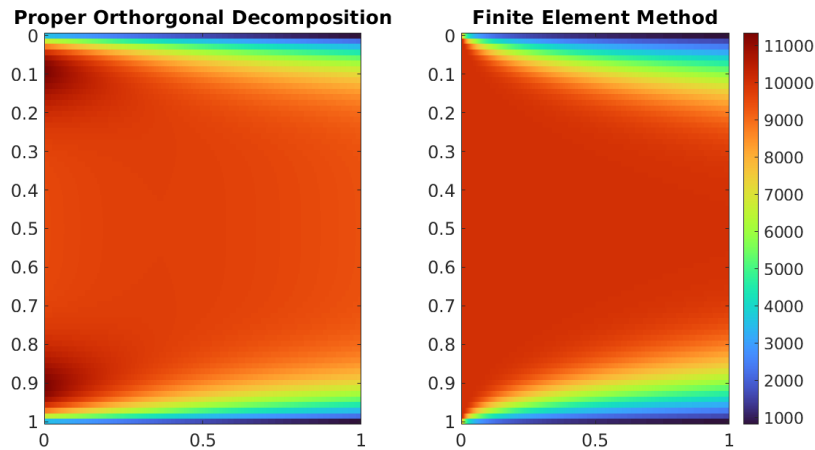


Figure 3.4.: FEM solution and POD approximation for heat equation

3.3. Balanced Truncation

Balanced truncation is a method for model order reduction. The goal of balanced truncation is to approximate a system using only the most relevant modes of the system. The difference to POD is that the modes are not selected by the variance they capture but by the controllability and observability of the modes. The first step to finding such an approximation is to find a coordinate transform.

3.3.1. Balanceing Coordinate Transform

The first step for generating a balanced truncation, is to find a orthonormal coordinate transform $x = Tz$. This yields a new system

$$\dot{z} = \hat{A}z + \hat{B}u \quad (3.21)$$

$$y = \hat{C}z + Du \quad (3.22)$$

$$\hat{A} = T^{-1}AT \quad \hat{B} = T^{-1}B \quad \hat{C} = CT. \quad (3.23)$$

The gramians of this ROM are obtainable by applying (2.76) and (2.75) to (3.23). This yields $\hat{W}_c = T^{-1}W_cT^{-*}$ and $\hat{W}_o = T^*W_oT$ with $T^{-*} := (T^{-1})^* := (T^*)^{-1}$. A requirement T has to satisfy is that it has to make the observability and controllability gramians of the ROM equal and diagonal

$$\hat{W}_c = \hat{W}_o = \Delta \quad (3.24)$$

$$\hat{W}_c\hat{W}_o = \Delta^2 \quad (3.25)$$

$$T^{-1}W_cW_oT = \Delta^2 \quad (3.26)$$

$$W_cW_oT = T\Delta^2. \quad (3.27)$$

Since Δ is a diagonal matrix, (3.27) is equal to the eigendecomposition of W_cW_o . Therefore T contains the eigenvectors of W_cW_o . The values in Δ are known as Hankel singular values. However T needs to be rescaled to make \hat{W}_c and \hat{W}_o equal. Here T_u denotes the unscaled eigenvectors of this eigendecomposition that yields gramians that are not equal to each other

$$T_u^{-1}W_cT_u^{-*} = \Delta_c \quad (3.28)$$

$$T_u^*W_cT_u = \Delta_o. \quad (3.29)$$

Scaling T_u by some diagonal matrix Δ_s results in $\Delta_c = \Delta_o$

$$\Delta_s = \Delta_c^{\frac{1}{4}}\Delta_o^{-\frac{1}{4}} \quad (3.30)$$

$$T = T_u\Delta_s. \quad (3.31)$$

Another important property of this transform is that the new coordinates are hierarchically ordered by observability and controllability. It can be shown by deriving some unit vector ζ that maximizes the controllability and observability

$$\zeta = \operatorname{argmax} \zeta^* W_c W_o \zeta \quad s.t. \|\zeta\|_2^2 = 1 \quad (3.32)$$

$$\frac{d}{d\zeta} \zeta^* W_c W_o \zeta - 2\lambda \zeta = 0. \quad (3.33)$$

As shown here [25] the remaining derivative can be solved in the following way

$$\frac{d}{dx} x^* A x = 2Ax. \quad (3.34)$$

This holds if A is symmetric. Here both W_c and W_o share the same set of eigenvectors (3.28) and (3.29), therefore they commute [26]. This means that the product of W_c and W_o is also symmetric [27]. Applying (3.34) to (3.33) yields

$$W_c W_o \zeta = \lambda \zeta. \quad (3.35)$$

Since λ is the Lagrange multiplier, it is a scalar. It is clear that ζ is an eigenvector. Since the eigenvalues in Δ contain information about how much each eigenvector gets scaled by multiplying it with $W_c W_o$, the eigenvectors can be ordered by controllability and observability.

3.3.2. Mode Truncation

Since the goal of balanced truncation is to find a reduced order model (ROM) of rank r that approximates the original system of rank n with $r \ll n$, it is necessary to truncate the balanced system. This yields the following system:

$$\frac{d\tilde{x}}{dt} = \tilde{A}\tilde{X} + \tilde{B}u \quad (3.36)$$

$$y = \tilde{C}\tilde{x} + \tilde{D}u. \quad (3.37)$$

The new state vector \tilde{x} is defined as

$$\tilde{x} = \begin{bmatrix} z_1 \\ \vdots \\ z_r \end{bmatrix} \quad \tilde{z} = \begin{bmatrix} z_{r+1} \\ \vdots \\ z_n \end{bmatrix} \quad z = \begin{bmatrix} \tilde{x} \\ \tilde{z} \end{bmatrix} \quad (3.38)$$

$$T = \begin{bmatrix} \Psi & T_t \end{bmatrix} \quad T^{-1} = S = \begin{bmatrix} \Phi^* \\ S_t \end{bmatrix}. \quad (3.39)$$

By substituting (3.38) and (3.39) into the system in (3.21) and (3.22) the system becomes

$$\frac{d}{dt} \begin{bmatrix} \tilde{x} \\ \tilde{z} \end{bmatrix} = \begin{bmatrix} \Phi^* A \Psi & \Phi^* A T_t \\ S_t A \Psi & S_t A T_t \end{bmatrix} \begin{bmatrix} \tilde{x} \\ \tilde{z} \end{bmatrix} + \begin{bmatrix} \Phi^* B \\ S_t B \end{bmatrix} u \quad (3.40)$$

$$y = \begin{bmatrix} C \Psi & C T_t \end{bmatrix} \begin{bmatrix} \tilde{x} \\ \tilde{z} \end{bmatrix} + D u. \quad (3.41)$$

However, the only relevant part of this system is

$$\frac{d\tilde{x}}{dt} = \Phi^* A \Psi \tilde{x} + \Phi^* B u \quad (3.42)$$

$$y = C \Psi \tilde{x} + D u \quad (3.43)$$

since this is the only part necessary to calculate \tilde{x} [28].

3.3.3. Computing Balanced Truncation

Since the gramians for controllability and observability are too expensive to compute for large systems, the so-called empirical gramians are used as an approximation. The empirical gramians are calculated by using the discrete-time system matrices from (2.65) and (2.66)

$$\mathcal{C}_d = \begin{bmatrix} B_d & A_d B_d & \cdots & d A_d^{m_o-1} B_d \end{bmatrix} \quad (3.44)$$

$$\mathcal{O}_d = \begin{bmatrix} C_d \\ C_d A_d \\ C_d A_d^{m_o-1} \end{bmatrix} \quad (3.45)$$

$$W_c^e = \mathcal{C}_d^* \mathcal{C}_d \quad (3.46)$$

$$W_o^e = \mathcal{O}_d^* \mathcal{O}_d \quad (3.47)$$

$$m_o, m_c \ll \text{rank}(A). \quad (3.48)$$

Now these empirical gramians can be used for obtaining the balancing coordinate transform [28].

3.3.4. State Space Representation from Heat Equation

A state space representation of that system must be found first to apply balanced truncation to the heat equation (2.6). Note that the system of ODEs resulting from FEM (2.39) resembles a state space representation

$$x := c \quad x_0 := c_0 \quad (3.49)$$

$$A := M^{-1} K \quad B := I. \quad (3.50)$$

Since the system is realized as a simulation, all states can be accurately measured $C := I$, and there is no feed through $D := 0_{qm}$. Now the already described steps for balanced truncation can be applied to the system.

Figure 3.5 shows a solution to heat equation using FEM and an approximation using BT with $u(x, t) = 0, x_0 = 10000^{70 \times 1}, n = 70, n_{approx} = 10$.

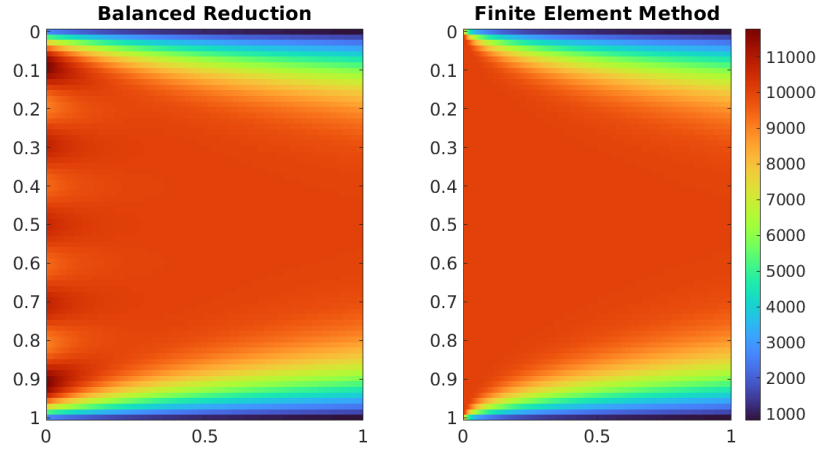


Figure 3.5.: FEM solution and BT approximation for heat equation

3.4. Modal truncation

3.4.1. Diagonal Canonical Form

A LTI system (A, B, C, D) with transfer function $G(s)$ can be written in the following way

$$I = \{1, 2, \dots, n\} \quad (3.51)$$

$$G(s) = D + \sum_{i \in I} \frac{\Phi_i}{s - \lambda_i}. \quad (3.52)$$

The set $\Lambda = \{\lambda_1, \dots, \lambda_n\}$ denotes the eigenvalues of the matrix A in state space. This resembles the partial fraction decomposition of $G(s)$ [29]. The residue Φ can be computed using the eigendecomposition of A and using the eigenvectors for a coordinate transform

$$AX = X\Delta \quad X\zeta = x. \quad (3.53)$$

The system matrices have to be transformed accordingly

$$\hat{A} = X^{-1}AX = \Delta \quad (3.54)$$

$$\hat{B} = X^{-1}B \quad \hat{C} = CX \quad (3.55)$$

$$\hat{D} = D. \quad (3.56)$$

Those transformed matrices are used to calculate the transfer function (2.74)

$$G(s) = CX(sI - \Delta)^{-1}X^{-1}B + D \quad (3.57)$$

$$= [Cx_1 \quad \dots \quad Cx_n] \text{diag} \left\{ \frac{1}{s - \lambda_1}, \dots, \frac{1}{s - \lambda_n} \right\} \begin{bmatrix} x_1^{-1}B \\ \vdots \\ x_n^{-1}B \end{bmatrix} + D \quad (3.58)$$

$$= \sum_{i \in I} \frac{c_i b_i^T}{s - \lambda_i} + D \Rightarrow \Phi_i = c_i b_i^T. \quad (3.59)$$

[30]

3.4.2. Optimal Modal Truncation

The goal of modal truncation is to find a subset of the indices I such that only r elements are contained in this subset

$$I_r \subseteq I, \quad |I_r| = r. \quad (3.60)$$

Using this subset as indices in (3.52), a truncation is obtained, yielding a system defined by a new transfer function $\hat{G}(s)$. The set I_r has to be chosen such that the error $\|G(s) - \hat{G}(s)\|_{H_2}$ becomes minimal. As shown in [29], other norms are also usable, but only the stated norm is used for simplicity. Furthermore, in case some $\lambda_i \in \Lambda$, $\text{Im}(\lambda_i) > 0$ is a complex number $i \in I_r$, the index of the corresponding complex conjugate eigenvalue has to be selected too, if $\lambda_j = \bar{\lambda}_i \in \Lambda \wedge i \in I_r \Rightarrow j \in I_r$. This yields the following optimization problem

$$G_\alpha(s) = D_\alpha + \sum_{i \in I} \alpha_i \frac{\Phi_i}{s - \lambda_i} \quad (3.61)$$

$$\min_{\alpha} \|G(s) - G_\alpha(s)\|_{s.t.} \quad \alpha^T \alpha = r. \quad (3.62)$$

With the following constraints

$$J = \{(\lambda_i, \lambda_j) \in I | \lambda_i \in \mathbb{C}, \text{Im}(\lambda_i) > 0, \lambda_i = \bar{\lambda}_j\} \quad (3.63)$$

$$a_{.,j} = -a_{.,l} = 1, \quad (i, j) \in J \quad (3.64)$$

$$A\alpha = 0. \quad (3.65)$$

Where $\alpha \in \{0, 1\}^n$ is some binary vector with $\alpha^T \alpha = r$ that represents the selection of indices. By defining the error of that system as

$$\epsilon_\alpha(s) = G(s) - G_\alpha \quad (3.66)$$

$$\|\epsilon_\alpha(s)\|_2^2 = \sum_{i,k \in I} (1 - \alpha_i) \frac{\text{trace}(\phi_i \phi_k^T)}{-\lambda_i - \lambda_k} (1 - \alpha_k) \quad (3.67)$$

$$\|\epsilon_\alpha(s)\|_2^2 = (1 - \alpha)Q(1 - \alpha) \quad (3.68)$$

$$q_{ij} = \frac{\text{trace}(\phi_i \phi_k^T)}{-\lambda_i - \lambda_k^*}. \quad (3.69)$$

This leads to a new optimization problem [29]

$$\min_{\alpha} \quad (1 - \alpha)Q(1 - \alpha) \quad (3.70)$$

$$s.t. \quad \alpha^T \alpha = r \quad (3.71)$$

$$A\alpha = 0. \quad (3.72)$$

3.4.3. Applying Modal Truncation to Heat Equation

As described in (3.3.4), the system matrices (A, B, C, D) can be obtained for the given heat equation. Now by applying (2.74) yields the corresponding transfer function $G(s)$. By calculating the partial fraction decomposition as described in section 3.4.1, the DCNF can be obtained. Since B and C are given by some identity matrix and D is a zero matrix, the upper error bound of the error in H_2 norm is given as [29]

$$\|\epsilon(s)\|_{H_2} \leq \sum_{i \in I_r^c} \frac{1}{\sqrt{-2 \text{Re}(\lambda_i)}}. \quad (3.73)$$

Since for stable systems $\text{Re}(\lambda) < 0 \forall \lambda \in \Lambda$ this upper bound can be expressed as follows with $\Lambda_\epsilon = \{\text{Re}(\lambda_i) | \lambda_i \in \Lambda, i \in I_r^c\}$

$$\|\epsilon(s)\|_{H_2} \leq \sum_{i \in I_r^c} \frac{1}{\sqrt{2|\text{Re}(\lambda_i)|}} \leq \frac{|I_r^c|}{\sqrt{2|\max(\Lambda_\epsilon)|}}. \quad (3.74)$$

To minimize this upper bound $|\max(\Lambda_\epsilon)|$ has to be maximized. This is achieved by selecting the entries of Λ_ϵ such that it contains the $n - r$ largest real parts of the eigenvalues in Λ . Figure 3.6 shows a solution to heat equation using FEM and an approximation using MT with $u(x, t) = 0, x_0 = 10000^{70 \times 1}, n = 70, n_{approx} = 10$.

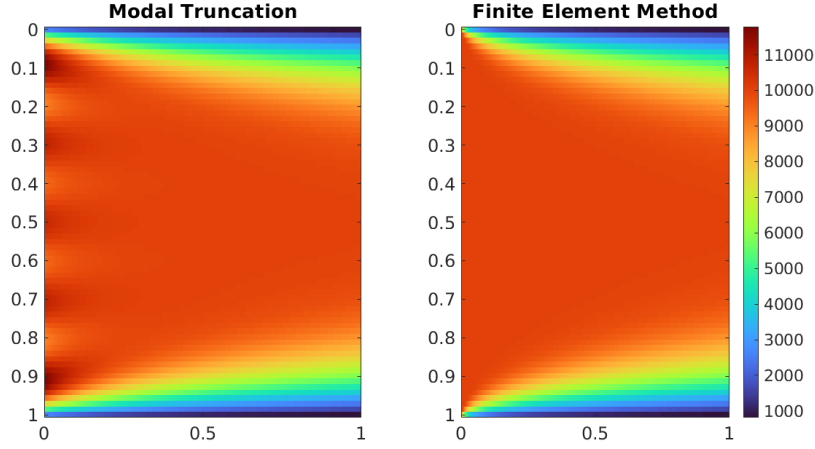


Figure 3.6.: FEM solution and MT approximation for heat equation

3.5. Hankel Norm Approximation

The Hankel Norm Approximation (HNA) aims to find a reduced order system that approximates a system G such that the error in the so-called Hankel norm becomes minimal. The Hankel norm is defined to be the largest Hankel singular value [31]

$$\|G(s)\|_H = \sigma_{max} = \sqrt{\lambda_{max}(W_c W_o)}. \quad (3.75)$$

Therefore the problem can be stated as follows

$$G_r = \operatorname{argmin} \|G - G_r\|_H. \quad (3.76)$$

3.5.1. System Spaces

For the following section it is necessary to define the four following system spaces: L_∞ , H_∞ , H_∞^- and $H_\infty^-(r)$.

$$L_\infty \quad G \in L_\infty \text{ iff } \sup_\omega \|G(i\omega)\| < \infty.$$

$$H_\infty \quad G \in H_\infty \text{ iff } \forall \lambda \in \mathbb{C}_-. \text{ Here } \lambda \text{ are the eigenvalues of } A.$$

$$H_\infty^- \quad G \in H_\infty^- \text{ iff } G(-s) \in H_\infty.$$

$$H_\infty^-(r) \quad G \in H_\infty^-(r) \text{ iff } G \in L_\infty \text{ and } \lambda = \lambda_+ \cap \lambda_- = \{\lambda_1, \dots, \lambda_n\} \text{ with } \lambda_o = \{\lambda_i \in \lambda \mid \lambda_i \in \mathbb{C}_{-o}\} \text{ and } |\lambda_-| \leq r.$$

3.5.2. Optimal Solution

A lower bound for $\min \|G - G_r\|_H$ is established by lemma 7.1 in [32]

$$\min \|G - G_r\|_H \geq \sigma_{r+1}. \quad (3.77)$$

Here σ_{r+1} is the $r + 1$ th largest Hankel singular value of G . Hence a system G_r is optimal if $\|G - G_r\|_H = \sigma_{r+1}$.

It is important to note that the Hankel norm can be related to the L_∞ norm through the Nehari Theorem

$$G \in H_\infty, \quad F \in H_\infty^-, \quad G - F \in L_\infty \quad (3.78)$$

$$\|G\|_H = \min_{F \in H_\infty^-} \|G - F\|_\infty. \quad (3.79)$$

Also, the Adamjan-Arov-Krein theorem has to be stated to find an optimal solution to the stated minimization problem

$$G \in H_\infty, \quad Q \in H_\infty^-(r), \quad G - Q \in L_\infty \quad (3.80)$$

$$\min_{Q \in H_\infty^-} \|G - Q\|_\infty = \sigma_{r+1}. \quad (3.81)$$

Suppose there is an optimal system $Q^* = G_r + F$ with $Q^* \in H_\infty^-(r)$, $G_r \in H_\infty$, $F \in H_\infty^-$. It has the following error bound

$$\|G - G_r\|_\infty = \|G - Q^* + F\|_\infty \leq \sigma_{r+1} + \|F\|_\infty. \quad (3.82)$$

If $\|F\|_\infty$ is small enough, the stable part of Q^* can be used as a reduced order model. It is also an optimal solution to (3.76) [33]

$$\|G - G_r\|_H = \min_{F \in H_\infty^-} \|G - G_r - F\|_\infty = \min_{Q \in H_\infty^-} \|G - Q\|_\infty = \sigma_{r+1}. \quad (3.83)$$

3.5.3. Constructing Q^*

The first step to construct an optimal system Q^* is to construct a balanced realization of the system $G = (A, B, C, D) \in H_\infty$ that is to be reduced, as described in section 3.3.1. Hence the gramians W_c and W_o are equal and diagonal

$$W_c = \begin{bmatrix} P_1 & 0 \\ 0 & \sigma_{r+1} I_l \end{bmatrix}, \quad W_o = \begin{bmatrix} Q_1 & 0 \\ 0 & \sigma_{r+1} I_l \end{bmatrix}. \quad (3.84)$$

Now G is partitioned in the following way

$$A = \begin{bmatrix} A_{11} & A_{12} \\ A_{21} & A_{22} \end{bmatrix}, \quad B = \begin{bmatrix} B_1 \\ B_2 \end{bmatrix}, \quad C = \begin{bmatrix} C_1 \\ C_2 \end{bmatrix}. \quad (3.85)$$

Also a unitary matrix U has to be defined such that $B_2 = -C_2^T U$ and $U^T U = I$. Further more a matrix $E_1 = P_1 Q_1 - \sigma_{r+1}^2 I$ is introduced.

Then a system $Q^* = (\hat{A}, \hat{B}, \hat{C}, \hat{D})$ can be defined [33]

$$\hat{A} = E_1^{-1}(\sigma_{r+1}^2 A_{11}^T + Q_1 A_{11} P_1 - \sigma_{r+1} C_1^T U B_1^T) \quad (3.86)$$

$$\hat{B} = E_1^{-1}(Q_1 B_1 + \sigma_{r+1} C_1^T U) \quad (3.87)$$

$$\hat{C} = C_1 P_1 + \sigma_{r+1} U B_1^T \quad (3.88)$$

$$\hat{D} = D - \sigma_{r+1} U. \quad (3.89)$$

3.5.4. Decomposition of Q^*

The final step is to decompose Q^* into two systems $G_r \in H_\infty, F \in H_\infty^-$. To achieve this, Q^* can be expressed in the diagonal canonical form described in section 3.4.1.

$$Q^* = D + \sum_{i=1}^r \frac{\phi_i}{s - \lambda_i}. \quad (3.90)$$

This can no be decomposed into three systems $K \in H_\infty, V \in H_\infty^-$ and \tilde{D} with

$$\text{Re}(\lambda_i) \in \mathbb{C}_o \forall i \in I_o. \quad (3.91)$$

$$K = \sum_{i \in I_-} \frac{\phi_i}{s - \lambda_i} \quad (3.92)$$

$$V = \sum_{i \in I_+} \frac{\phi_i}{s - \lambda_i} \quad (3.93)$$

$$\tilde{D} = \hat{D}. \quad (3.94)$$

Since \tilde{D} is some constant, it does not have any poles. Therefore $K + D \in H_\infty$ and $V + D \in H_\infty^-$ which leads to two different decompositions $Q^* = (K + \tilde{D}) + V$ and $Q^* = K + (V + \tilde{D})$. From (3.82), it is clear that $\|F\|_\infty$ has to be as small as possible to minimize the error bound. It can be shown that $Q^* = (K + \tilde{D}) + V$ is the optimal decomposition. Suppose $Q^* = K + (V + \tilde{D})$ was the optimal decomposition, then the corresponding lower bound has to be smaller

$$\|G - K\|_\infty \leq \|G - (K + \tilde{D})\|_\infty \quad (3.95)$$

$$\sigma_{r+1} \|V + \tilde{D}\|_\infty \leq \sigma_{r+1} \|V\|_\infty \quad (3.96)$$

$$\|V + \tilde{D}\|_\infty \leq \|V\|_\infty + \|\tilde{D}\|_\infty \geq \|V\|_\infty \quad (3.97)$$

$$\Rightarrow \|G - K\|_\infty \geq \|G - (K + \tilde{D})\|_\infty. \quad (3.98)$$

Therefore $G_r = K + D$ and $F = V$.

3.6. Modal Truncation is Equal to Balanced Truncation

The results for BT and MT are the same since $B = C$ and A is symmetric. Remember that $A^{n \times n} = M^{-1}K$ where both K and M are symmetric, hence A is symmetric [27]. The eigenvectors of a symmetric matrix are mutually orthogonal [34]. Therefore the eigendecomposition of A is

$$AX = X\Delta. \quad (3.99)$$

The eigenvalues of a symmetric matrix are real. It is assumed that $\Delta = \text{diag}(\lambda_1, \dots, \lambda_n)$ with $\lambda_1 \geq \lambda_2 \geq \dots \geq \lambda_n$. where $XX^T = X^T X = I$. By applying $x = X\zeta$ to the system, the system becomes

$$\dot{\zeta} = \Delta\zeta + X^T u(t) \quad (3.100)$$

$$\zeta = X\zeta + Du(t). \quad (3.101)$$

The gramians of that system are

$$W_c = \lim_{t \rightarrow \infty} \int_0^t e^{\Delta\tau} I e^{\Delta\tau} d\tau \quad (3.102)$$

$$= \lim_{t \rightarrow \infty} \int_0^t e^{2\Delta\tau} d\tau \quad (3.103)$$

$$= \lim_{t \rightarrow \infty} (e^{\Delta t} - I) \Delta^{-1} \quad (3.104)$$

$$W_o = \lim_{t \rightarrow \infty} \int_0^t e^{\Delta\tau} I e^{\Delta\tau} d\tau \quad (3.105)$$

$$= \lim_{t \rightarrow \infty} \int_0^t e^{2\Delta\tau} d\tau \quad (3.106)$$

$$= \lim_{t \rightarrow \infty} (e^{\Delta t} - I) \Delta^{-1}. \quad (3.107)$$

Therefore $W_c = W_o$, where W_c and W_o are diagonal for stable systems. Since the transfer of heat is a stable process, it is assumed that the according system is stable [35]

$$W_c = W_o = \lim_{t \rightarrow \infty} (e^{\Delta t} - I) \Delta^{-1} \quad (3.108)$$

$$= -\Delta^{-1} \quad (3.109)$$

$$W_C = W_o = \begin{bmatrix} \frac{-1}{\lambda_1} & 0 & \dots & 0 \\ 0 & \frac{-1}{\lambda_2} & 0 & \vdots \\ \vdots & 0 & \ddots & \vdots \\ 0 & 0 & \dots & \frac{-1}{\lambda_n} \end{bmatrix}. \quad (3.110)$$

This shows that the eigenvectors of A satisfy the conditions for balancing transformation T in section 3.3. Since the eigenvalues are all negative and real the order $\lambda_{11} \geq \lambda_{22} \geq \dots \lambda_{nn}$ applies. This enables the mode truncation described in section 3.3

$$\tilde{x} = \begin{bmatrix} \zeta_1 \\ \vdots \\ \zeta_r \end{bmatrix} \quad \tilde{z} = \begin{bmatrix} \zeta_{r+1} \\ \vdots \\ \zeta_n \end{bmatrix} \quad z = \begin{bmatrix} \tilde{x} \\ \tilde{z} \end{bmatrix} \quad (3.111)$$

$$X = \begin{bmatrix} X_r & X_{n-r} \end{bmatrix} \quad X^{-1} = \begin{bmatrix} X_r^* \\ X_{n-r} \end{bmatrix} \quad (3.112)$$

$$\frac{d\tilde{x}}{dt} = \Delta_r \tilde{x} + X_r^{-1} u \quad (3.113)$$

$$y = X_r \tilde{x} + D u. \quad (3.114)$$

The transfer function of that system is

$$G(s) = X_r(sI - \Delta_r^{-1})X_r^T + D = X_r \text{diag}\left(\frac{1}{s - \lambda_1}, \dots, \frac{1}{s - \lambda_r}\right)X_r^T + D \quad (3.115)$$

$$= \sum_{i=1}^r \frac{1}{s - \lambda_i} + D. \quad (3.116)$$

This resembles the DCNF of that system where the terms corresponding to the $n - r$ smallest eigenvalues are truncated. As shown in section 3.4.3, this is the optimal modal truncation. Therefore modal truncation and balanced truncation yield the same system.

4. Implementation

The implementation of the discussed methods for solving the heat equation and for model order reduction was done in Matlab. Matlab was chosen as the programming language because it natively features matrix multiplication which finds heavy use in the previously mentioned methods. The second reason for this selection is that ToolBoxes already implement certain model order reduction methods, such as MORLAB [36] or MOR toolbox [37]. The following figure 4.1 shows the class diagram of the implementation.

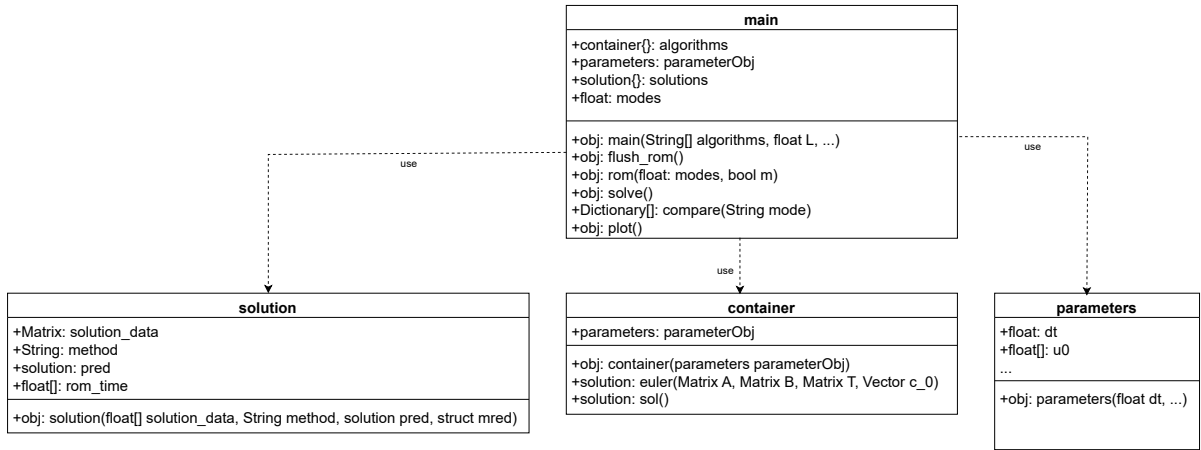


Figure 4.1.: Class diagram main

4.1. Class main

The class main is responsible for generating the finite element solution, model order reduction steps, and plotting and comparing the results as well. The process can be seen in the following flow chart:

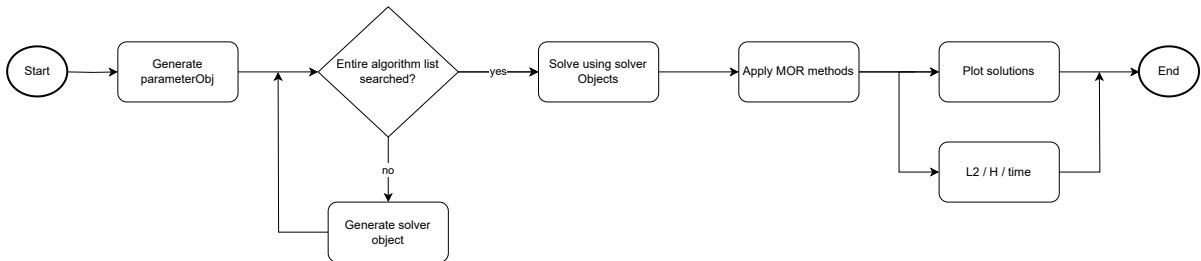


Figure 4.2.: Flow chart of main class

The first step is to generate a parameter object. The parameter object stores all parameters to increase the transparency and robustness of the program. The second step is to iterate the array of stated algorithms to solve the heat equation. The options are to solve the heat equation using the finite element method section 2.2. After all solver objects have been generated, the according solutions are computed. The final step is to display the solutions or return the $L2$, H_∞ error of each ROM. The processing time can be returned as well.

4.2. Class solution

The solution class is mainly responsible for storing solutions with some metadata. This metadata consists of the method used to generate the stored solution, its predecessor, and

computing time. The predecessor is important to plot reduced order model solutions side by side with the original finite element solution. The processing time is stored in an array that typically stores ten measurements.

4.3. Class parameters

The parameters class stores all parameters that have to be distributed. They are all encapsulated within this class to make distribution and modification easier.

4.4. Class container

The container class functions like an abstract class. It implements some methods, such as *euler()*, to avoid redundancy within its child classes. This method takes some matrices and a vector of initial conditions and generates a solution object that stores the solution generated using an Euler scheme. If the solution to a ROM is computed, it has to be transformed. This step is also done here. For this class, no objects are invoked.

Algorithm 1 Solve a system of ODEs using Euler scheme

Input

- A matrix of system
- B matrix of system
- T Coordinate transform to retrieve full state approximation of solution
- c_0 Initial condition

Output

- solution object

```

1: procedure EULER
2:    $C \leftarrow [Tc_0]$ 
3:    $j \leftarrow 2$ 
4:   for  $t = dt$  to  $T$  do
5:      $c_n \leftarrow dtAc_0 + dtBh(:, j) + c_0$ 
6:      $c_0 \leftarrow c_n$ 
7:      $C(:, j) \leftarrow Tc_0$ 
8:      $j = j + 1$ 
9:   end for
10:   $\text{sol} = \text{solution}(C, "", 0, 0)$ 
11: end procedure
```

Here dt , T and h are provided by the parameter object, dt is the time step, T is the time limit to which the solution is to be computed, and h is the input to the system. Since this method is common among all classes derived from the container class, only the solution is

stored in the solution object. The remaining fields of that object are set in the child class after the object has been returned. Those classes derived from the container class can be seen in figure 4.3.

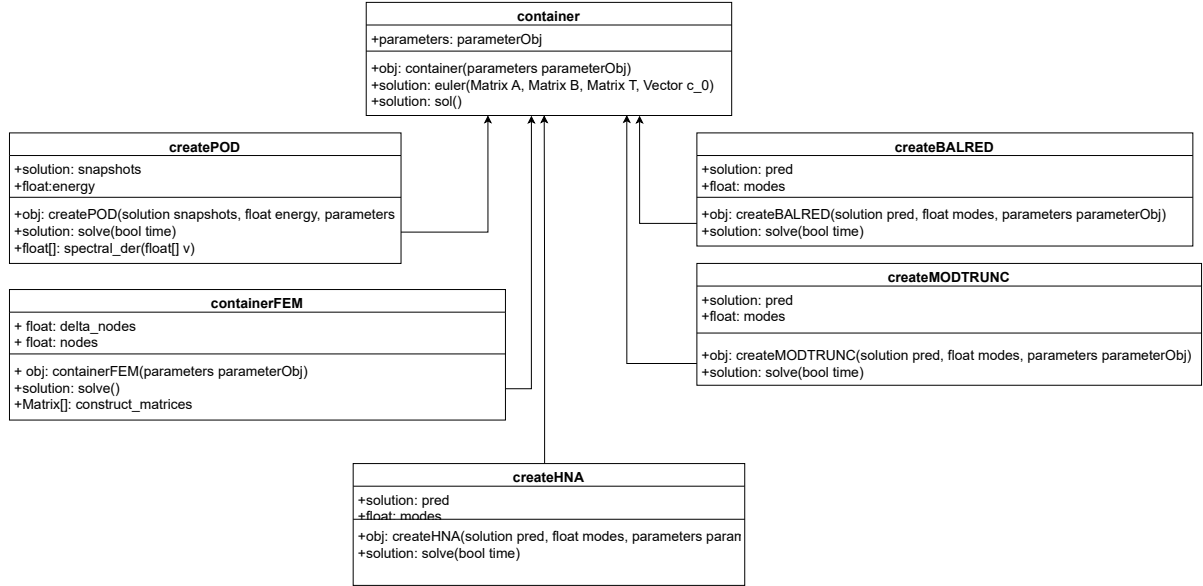


Figure 4.3.: Class diagram of MOR and FEM implementation

4.5. Class createBALRED, createMODTRUNC and createHNA

Those classes are fairly simple. MORLAB implements the actual model order reduction methods except for proper orthogonal decomposition. Hence the according function is called and provided with the right set of parameters, and the ROM gets generated. After that, a solution is generated using the previously described *euler()* method. For time measurements, the ROM gets generated ten times, and for each cycle, the time is stopped. To save time, no solutions are generated in this case.

4.6. Class containerFEM

The class containerFEM generates a solution and the state space representation of the system using the finite element method. FEM is implemented as shown in figure 4.4.

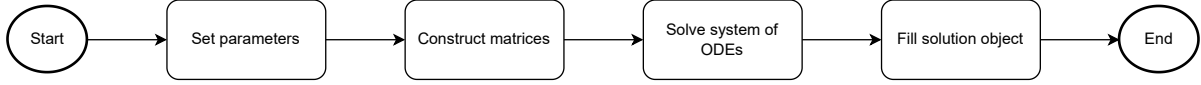


Figure 4.4.: Flow chart for FEM class

The first step is to set the parameters. After that, the matrices discussed in section 2.2 are being constructed. The next step is to solve the resulting system of ODEs and pass the solution to a solution object.

4.6.1. Construct Matrices

As defined in (2.34) the matrices K and M have to be constructed. This is done by the following method:

Algorithm 2 Construct matrices K and M

Input

Output

$[K, M]$

```

1: procedure CONSTRUCTMATRICES
2:    $ii \leftarrow \frac{2}{3}\Delta nodes$ 
3:    $ij \leftarrow \frac{1}{6}\Delta nodes$ 
4:    $F \leftarrow \text{zeros}(nodes, 1)$ 
5:    $M \leftarrow \text{zeros}(nodes)$ 
6:   for  $i = 1$  to  $nodes$  do
7:      $K(i, i) \leftarrow \frac{-2}{\Delta nodes}$ 
8:      $M(i, i) \leftarrow ii$ 
9:     if  $i - 1 > 1$  then
10:       $K(i, i - 1) \leftarrow \frac{1}{\Delta nodes}$ 
11:       $M(i, i - 1) \leftarrow ij$ 
12:     end if
13:     if  $i + 1 < nodes + 1$  then
14:       $K(i, i + 1) \leftarrow \frac{1}{\Delta nodes}$ 
15:       $M(i, i + 1) \leftarrow ij$ 
16:     end if
17:   end for
18:   return  $[K, M]$ 
19: end procedure

```

4.6.2. Solve System of ODEs

The resulting system of ODEs is solved using the implementation of the Euler scheme in the container class. After the solution is generated, the returned solution object gets filled with the according metadata and returned.

4.7. Class createPOD

The implementation of proper orthogonal decomposition is not included in the used MORLAB package. Therefore it is implemented in the createPOD class. The first step is constructing the matrix Φ as described in section 3.2. This is done by computing the SVD of the provided FEM solution and truncating the resulting U matrix, such that the r most dominant modes are included. In the following step, the transformed initial condition and the spacial derivative of Φ are computed. The spatial derivative is computed using the spectral derivative. In the last step, the resulting system of ODEs is solved using the implemented Euler scheme, and the resulting solution object is filled.

Algorithm 3 Create POD

Input

X Snapshot matrix
time boolean

Output

solution object

```
1: procedure SOLVE
2:   if time then
3:     for  $i = 1$  to 10 do
4:        $T1 = tic$ 
5:        $[U, S, V] \leftarrow SVD(X, "econ")$ 
6:        $\Phi = U(:, 1:r)$ 
7:       for  $i = 1$  to  $r$  do
8:          $\Phi_{xx}(:, i) \leftarrow spectral\_der(\Phi(:, i))$ 
9:         rom_time(i)  $\leftarrow T1 - toc$ 
10:      end for
11:    end for
12:    sol  $\leftarrow$  solution(NaN, "POD",  $X$ , NaN)
13:    sol.rom_time  $\leftarrow$  rom_time
14:  end if
15:   $[U, S, V] \leftarrow SVD(X, "econ")$ 
16:   $\Phi = U(:, 1:r)$ 
17:  for  $i = 1$  to  $r$  do
18:     $\Phi_{xx}(:, i) \leftarrow spectral\_der(\Phi(:, i))$ 
19:  end for
20:  sol  $\leftarrow euler(\alpha \Phi^T \Phi_{xx}, \Phi^T, \phi, \Phi^T u_0)$ 
21:  rom = struct("A",  $\alpha \Phi^T \Phi_{xx}$ , "B",  $\Phi^T$ , "C",  $\Phi$ , "D", parameterObj.D);
22:  sol.method = "Proper Orthogonal Decomposition"
23:  sol.pred =  $X$ , sol.reduced_model = rom
24: end procedure
```

From lines three to fifteen, there is some redundancy. This section is meant to measure the processing time of POD without generating a solution. The time measurements are stored in a solution object. The spectral derivative is implemented in the following way.

Algorithm 4 Compute spectral derivative

Input v Vector **Output** v' Derivative of v

```
1: procedure SPECTRAL_DER()  
2:    $v' \leftarrow -k^2 \text{fft}(v)$   
3: end procedure
```

Here k are the wave numbers, and all multiplication is element-wise multiplication.

4.8. Measurements

In the next chapter, some measurements are taken to gain information about the performance and error of each method. Therefore three sets of measurements are taken. The first two are the $L2$, and H_∞ errors of the results, and the last one is the processing time. Further details are in the according chapter.

4.8.1. $L2$ error

The $L2$ error gets determined in the *compare()* method in the main class. It gets computed in the following way.

$$E2 = \|S - S'\|_F \quad (4.1)$$

Here S is the solution of the ROM, and S' is the original FEM solution.

4.8.2. H_∞ error

The H_∞ error also gets determined in the *compare()* method in the main class.

$$H = \|S - S'\|_{H_\infty} \quad (4.2)$$

Here S is the transfer function of the ROM, and S' is the transfer function of the original FEM system.

4.8.3. Processing time

As already mentioned, the processing time gets determined in the according container class. It gets passed through the *compare()* method in the main class.

5. Comparison of MOR Methods

The previously mentioned methods for model order reduction will be compared regarding time domain error, frequency domain error, and computational speed. The time domain error will be obtained by comparing the FEM solution to a given approximation. To get insights into the frequency domain error, the error system of a reduced-order model will be analyzed. The computational speed will be determined by measuring the time it takes to generate a ROM. Here it is assumed that the implementations provided by MORLAB are programmed sufficiently effectively. For testing, the following parameters are used

$$\alpha = 0.1, \quad T = 1, \quad L = 1 \quad (5.1)$$

$$n = 100, \quad n_t = 10^4. \quad (5.2)$$

These values are chosen such that it yields results promptly. Especially n_t and α are important for the stability of the Euler scheme. If n_t is too small or α too large, the Euler scheme becomes unstable. Choosing n_t too large leads to larger time and memory consumption. There was no exact method for determining the parameters in this way.

5.1. Time Domain Error

The time domain error will be defined as $\epsilon = Y - \hat{Y}$ where Y and \hat{Y} denote the matrices storing the output of the systems G and G_r . Since the output matrices are usually rather large, it is impractical to use ϵ directly. Therefore $\|\epsilon\|_F$ will be considered. The error is measured using the Frobenius norm to get a measure of the error that respects all data points. Here two aspects are interesting. There will be two different initial conditions considered. The first one is $x(0, x) = 1$. It is chosen in this way to display the workings of the boundary condition. If there were no boundary conditions, for a constant initial condition, the system would never cool down since $\frac{\partial^2 u}{\partial x^2} = 0$ (2.6) at every point in time. This only holds if there is no input to the system. Therefore $u(t) = 0$, where u denotes the systems input. The second initial condition is $x(0, x) = \sin(\frac{2\pi}{L}x)$ with random input. The initial condition is sinusoidal since it is easy to approximate.

5.1.1. Proper Orthogonal decomposition

Figure 5.1 shows the L_2 error of the solution obtained by the POD model.

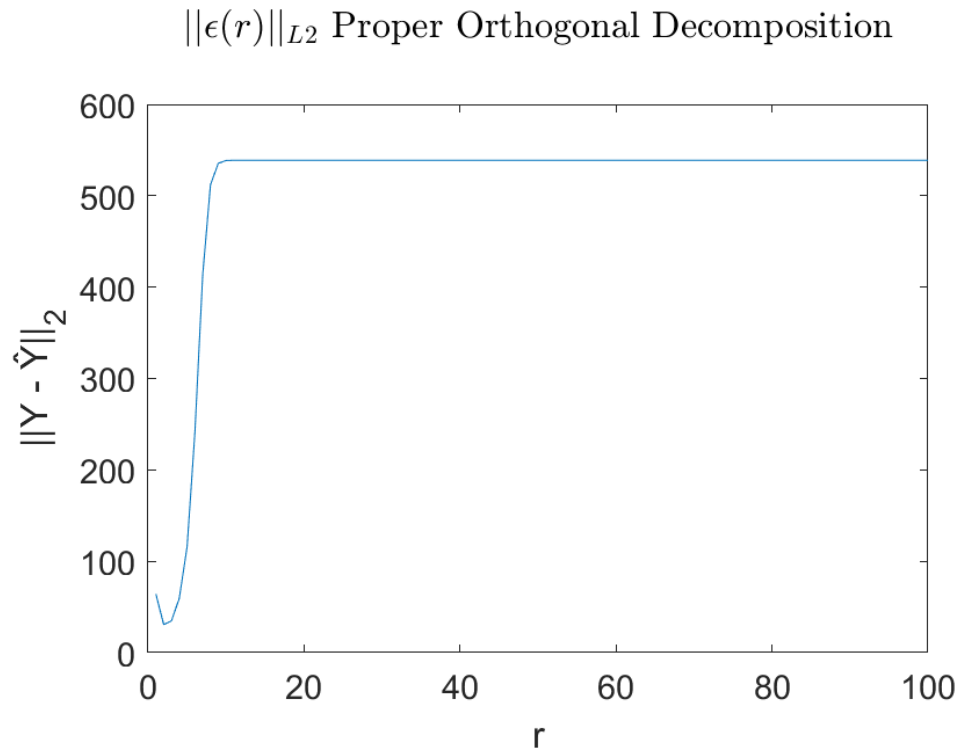


Figure 5.1.: L2 Error Proper Orthogonal Decomposition $x(0, x) = 1$

It is visible that the error is minimal at $r = 2$. This is to be expected since low variance modes will also be included for large r . Figure 5.2 shows that the first two modes capture the most variance with roughly 96% combined. It is also visible that all the remaining modes combined only capture 4%.

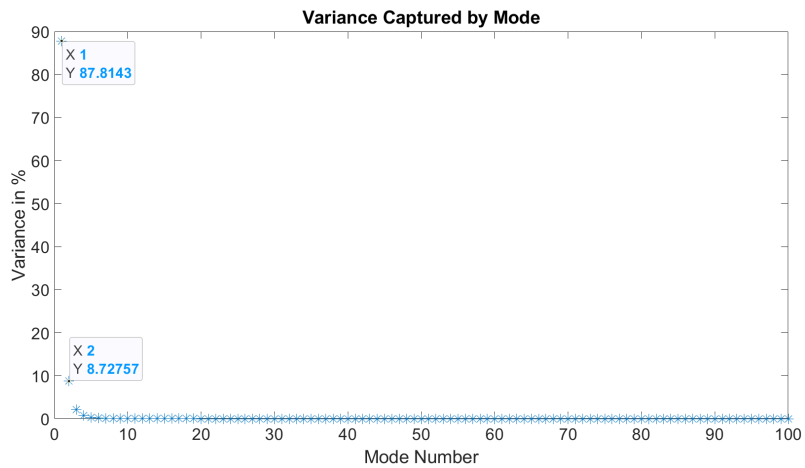


Figure 5.2.: Variance of POD Modes

In this case, the low variance modes introduce error since the initial condition is poorly approximated using orthogonal basis vectors. This can be seen in figure 5.3.

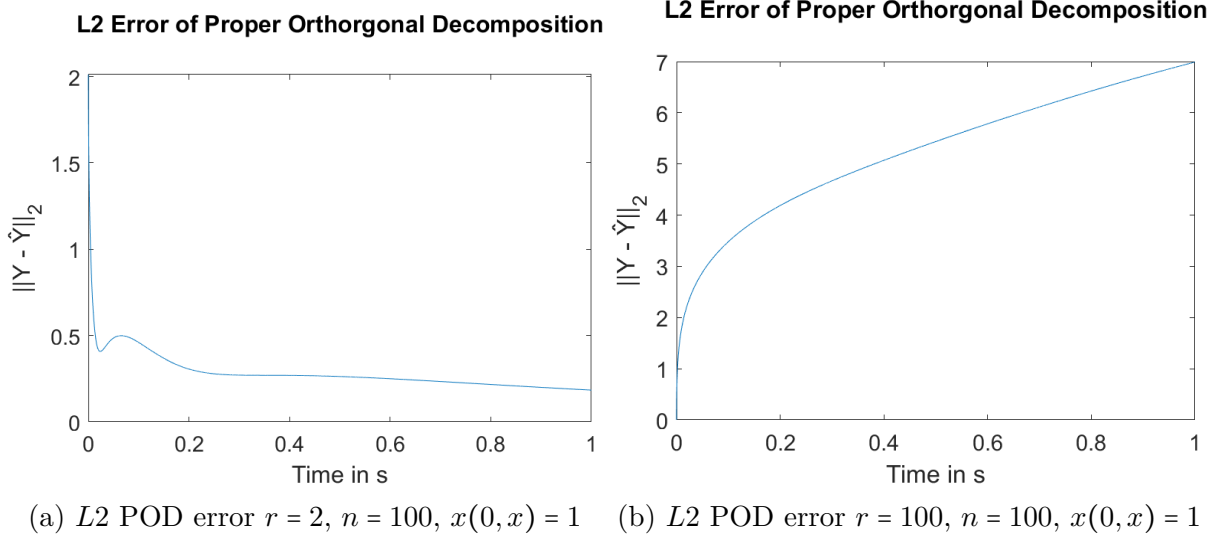


Figure 5.3.: $L2$ POD error $n = 100$, $x(0, x) = 1$

The $L2$ error for $r = 2$ can be seen on figure 5.3a. Here for $t = 0$, the error is the largest and then drops off quickly and seems to converge to roughly 0.3, whereas the error on figure 5.3b for $r = 100$ is almost zero at $t = 0$ and diverges. This problem does not only apply to the initial condition. This problem occurs if the snapshot matrix contains vectors that are poorly approximated using orthogonal basis vectors.

Figure 5.4 shows the $L2$ error of POD using with $x(0, x) = \sin(\frac{2\pi}{L}x)$. The low variance modes do not introduce error. They even lower the error, which is generally lower.

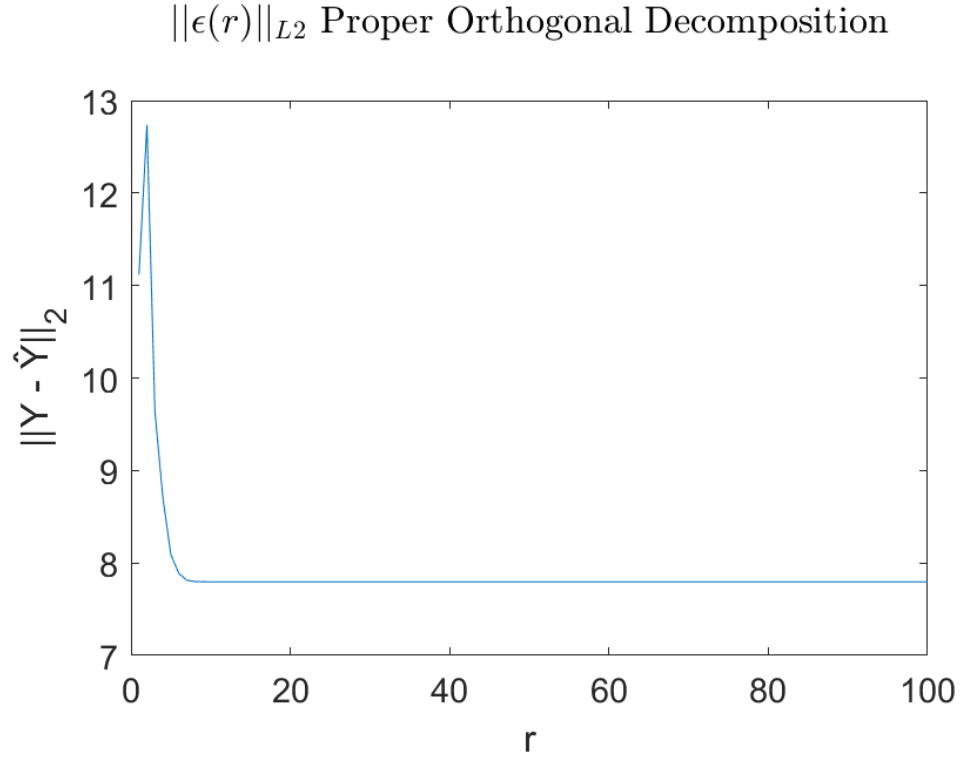


Figure 5.4.: L2 Error Proper Orthogonal Decomposition $x(0, x) = \sin(\frac{2\pi}{L}x)$

Another difference is that for $x(0, x) = \sin(\frac{2\pi}{L}x)$ the error distribution over time does not differ as much for $r = 100$ and $r = 2$. This can be observed in figure 5.5a and 5.5b.

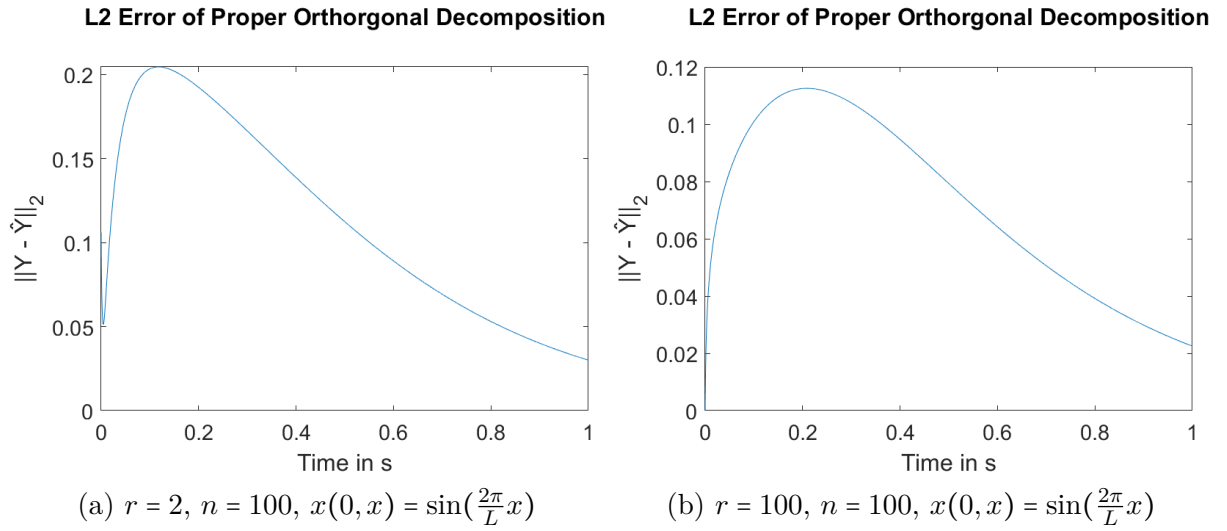


Figure 5.5.: L2 POD error

5.1.2. Modal Truncation

Figure 5.6a shows the L_2 error of the ROM obtained by Modal truncation.

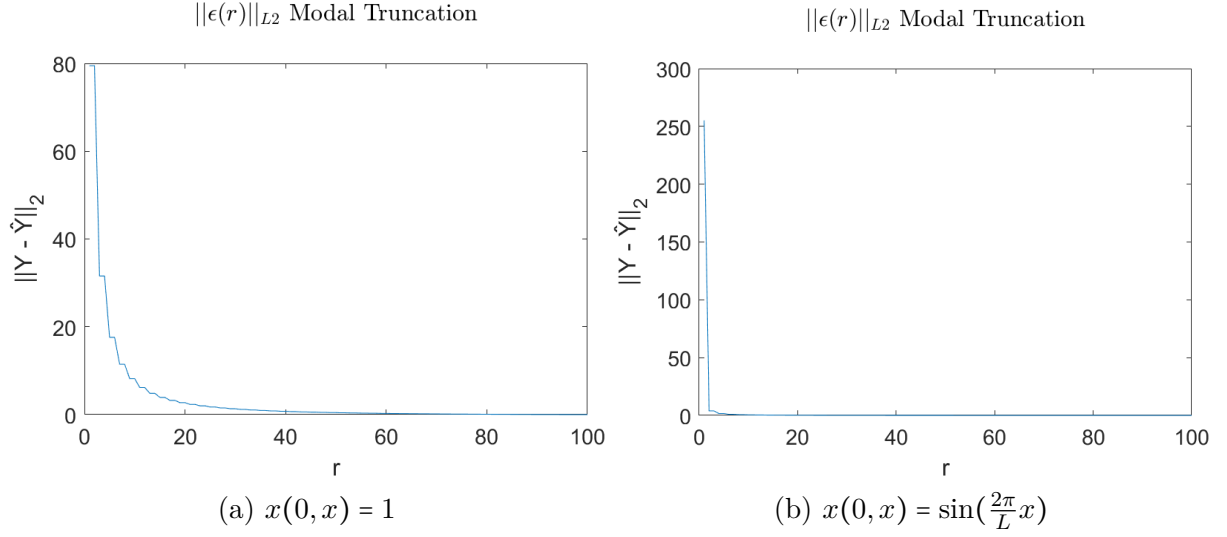


Figure 5.6.: L2 Error Balanced Truncation

It shows that the error converges to zero as r increases. This is to be expected since as r increases, G_r becomes closer to G . For $x(0, x) = \sin(\frac{2\pi}{L}x)$, the error starts significantly higher but decays even faster, as it can be seen in figure 5.6b.

5.1.3. Balanced Truncation

Figure 5.7a shows the L_2 error of the ROM obtained by Balanced truncation.

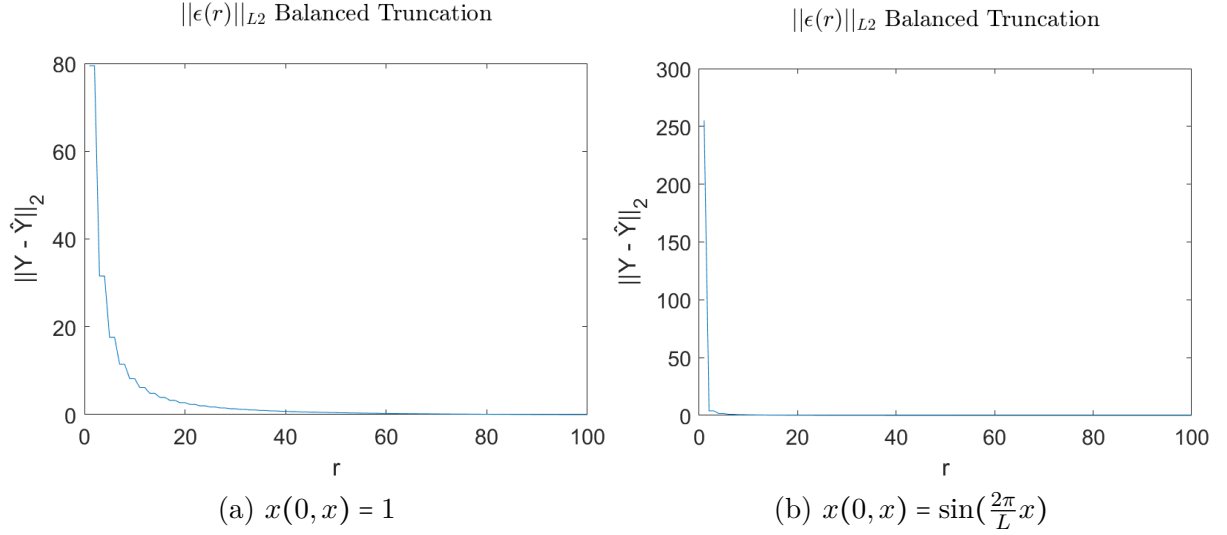


Figure 5.7.: L_2 Error Balanced Truncation

It shows that the error converges to zero as r increases. This is to be expected since as r increases, G_r becomes closer to G . As expected, the results for Modal truncation and Balanced truncation are the same.

5.1.4. Hankel Norm Approximation

Figure 5.8a shows the L_2 error of the output generated by the HNA model. It is striking that the model does not generate usable output for $r > 34$. This is because, for the chosen settings, the used Euler scheme does not converge for $r > 34$. Decreasing Δt yields results for $r > 34$, but it becomes prohibitively expensive to compute.

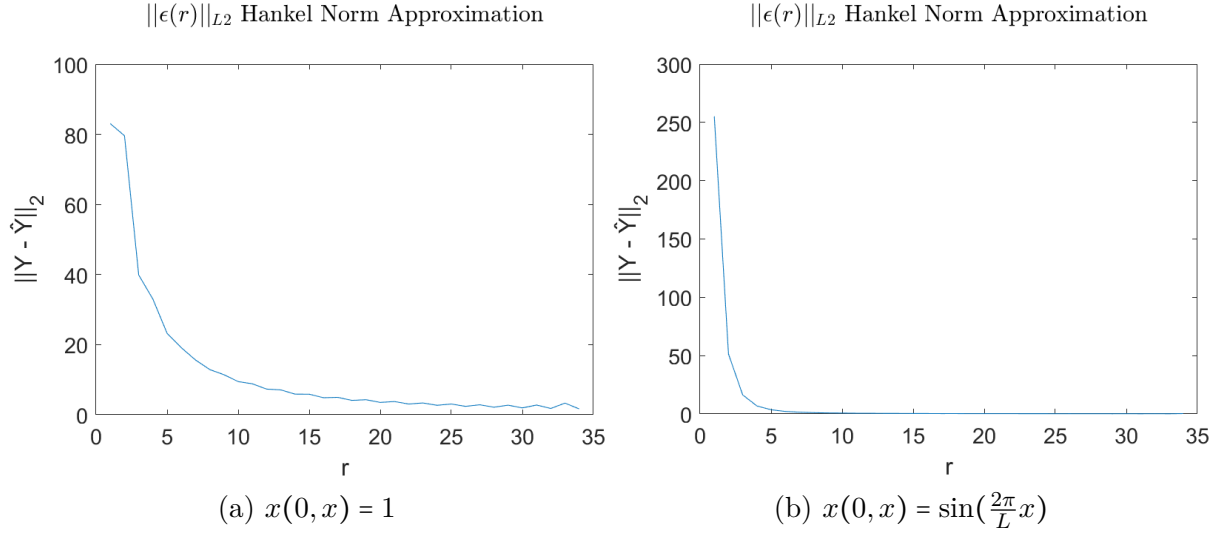


Figure 5.8.: L_2 Error Hankel Norm Approximation

It is noticeable that similar to BT and MT, the error for $x(0, x) = \sin(\frac{2\pi}{L}x)$ starts higher than for $x(0, x) = 1$ and then decays quite fast.

5.1.5. Comparison of Time Domain Error

Figure 5.9 shows the measured L_2 error plotted as a box plot to compare them. Since the range of the data is too large to plot them in this way, the data is transformed using \log_{10} . This results in the problem that zeros cannot be expressed. It is the case for Modal truncation at $r = 100$.

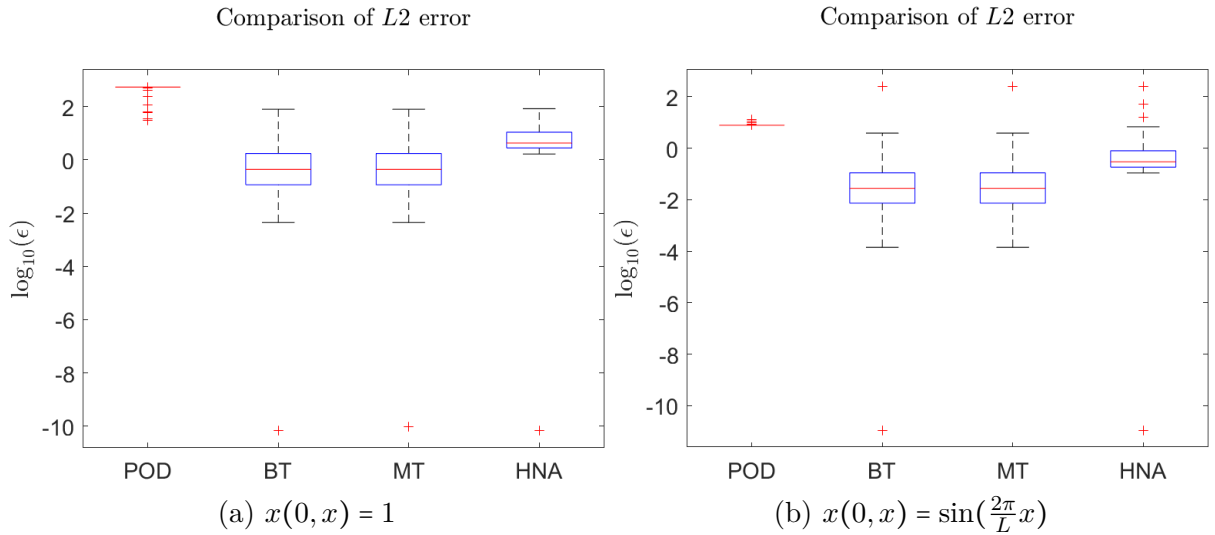


Figure 5.9.: Box Plot of L_2 Error

It is noticeable that the relative difference between each of the methods stays roughly the same for both initial conditions. As expected, all methods' error is generally higher for $x(0, t) = 1$. The box for POD has the lowest IQR while having the largest log error, meaning that the error of POD converges the fastest but does not converge to zero. Keep in mind that the seemingly large IQR of the error of MT and BT is small because the log error is depicted. Therefore the error of MT and BT converge faster than the one of HNA, while the error is smaller in general. Therefore BT and MT are the best choices when considering $L2$ time domain error.

5.2. Frequency Domain Error

The frequency domain error for $G_\epsilon = G - G_r$ will be determined using the H_∞ norm. For a MIMO system, this is the maximum singular value of the frequency response of the transfer matrix. It can be interpreted as the maximum gain from the i^{th} input to the i^{th} output [38]. The $H2$ cannot be used to get a measure of the error since the ROM that HNA yields has a nonzero feedthrough matrix, therefore $\|G_\epsilon\|_{H2}$ is infinite.

5.2.1. Proper Orthogonal Decomposition

Since the ROM obtained by POD is derived from a solution of the full-state system, it is dependent on the initial condition. Therefore the frequency domain error is also dependent on the initial condition. This can be seen in figure 5.10a and figure 5.10b. They differ from each other. For $x(0, x) = 1$ there are two distinct spikes at $r = 49$ and $r = 63$. The reason for them is unclear. However, the larger one is three orders of magnitude higher than the peak in the H_∞ error for $x(0, x) = \sin(\frac{2\pi}{L}x)$. This peak is not depicted in figure 5.10b since it is one single data point that is 14 orders of magnitude higher than the remaining data points. The peaks in figure 5.10a are not removed since the remaining data points are also large.

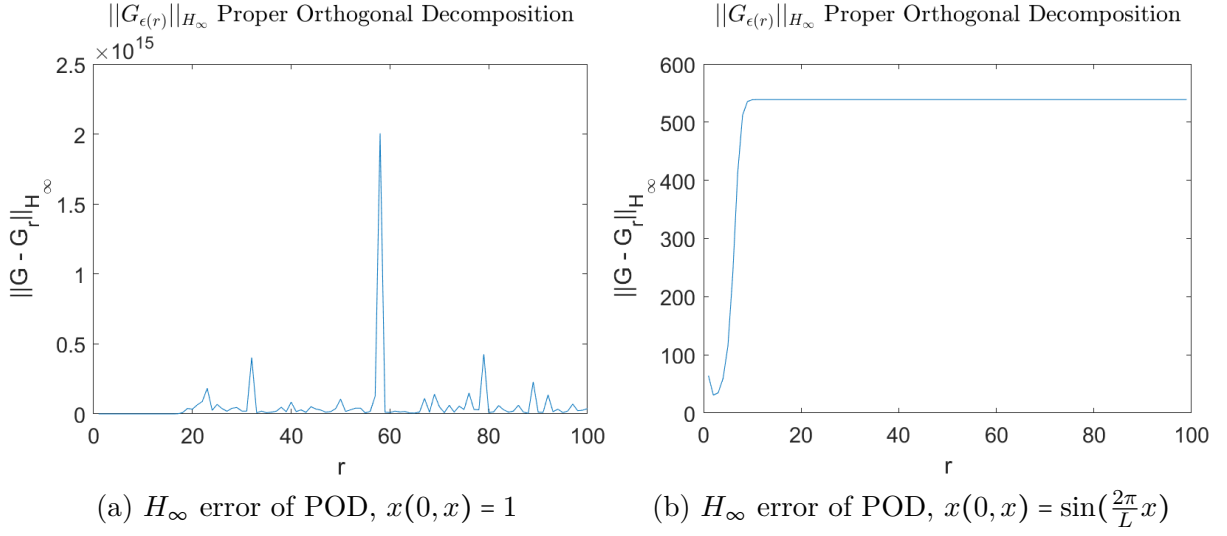


Figure 5.10.: H_∞ error of POD

In general the error in frequency domain is larger for $x(0, x) = 1$ than for $x(0, x) = \sin(\frac{2\pi}{L}x)$. This matches the behavior of the time domain error.

5.2.2. Modal Truncation and Balanced Truncation

The frequency domain error of Modal truncation and Balanced truncation is independent of the initial condition. For small r , it is comparably large and converges towards zero as r gets larger. As expected, the results of Balanced truncation and Modal truncation are the same as figure 5.11 shows.

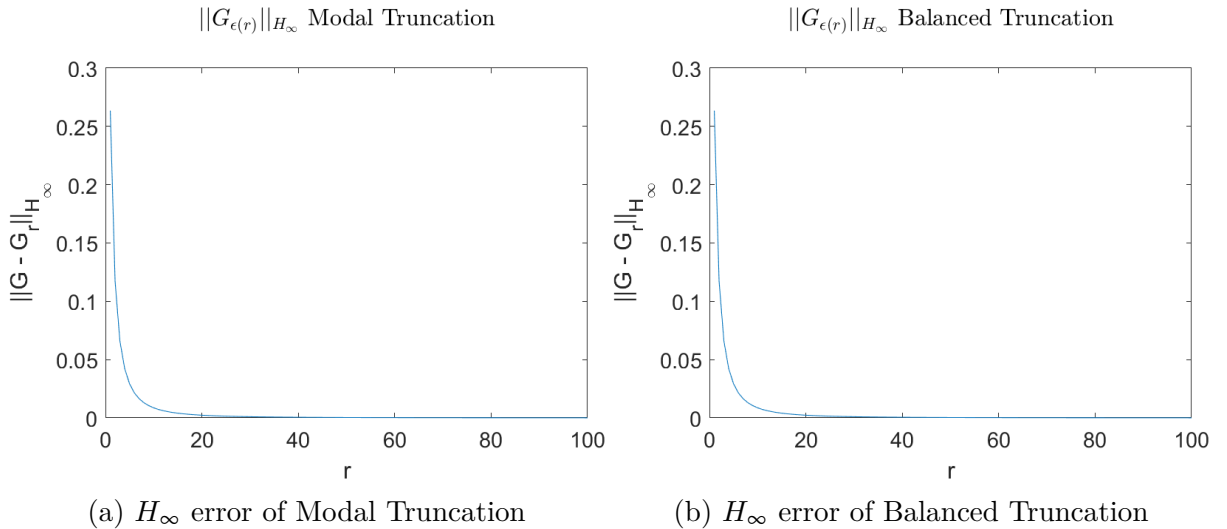


Figure 5.11.: H_∞ error of Balanced Truncation and Modal Truncation

5.2.3. Hankel Norm Approximation

Figure 5.12 shows the frequency domain error of HNA. Similar to BT and MT, the error is large for small r and decays as r gets larger. However, the error overall is smaller than for BT and HNA.

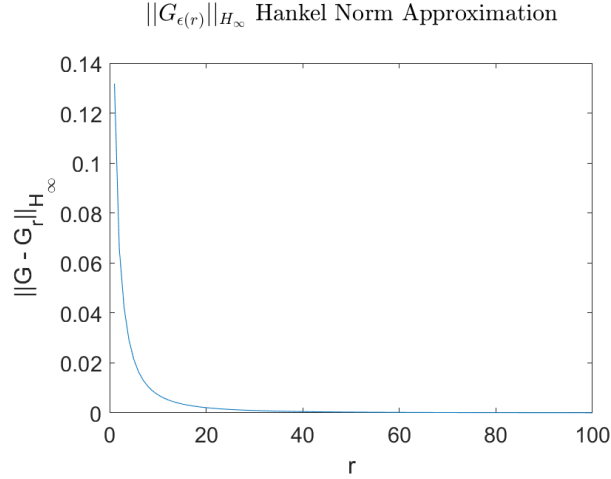


Figure 5.12.: H_{∞} error of Hankel Norm Approximation

5.2.4. Comparison of Frequency Domain Error

To compare the results directly, the error of the ROMs for all r are plotted using a box plot. However, the error is not directly used because of some large peaks in the data, which would render the plot unreadable. Instead, the \log_{10} of each data point is taken. This is possible since all data points are strictly positive. Therefore the order of the data points is preserved while lowering the range between outliers. The box plot can be seen in figure 5.13.

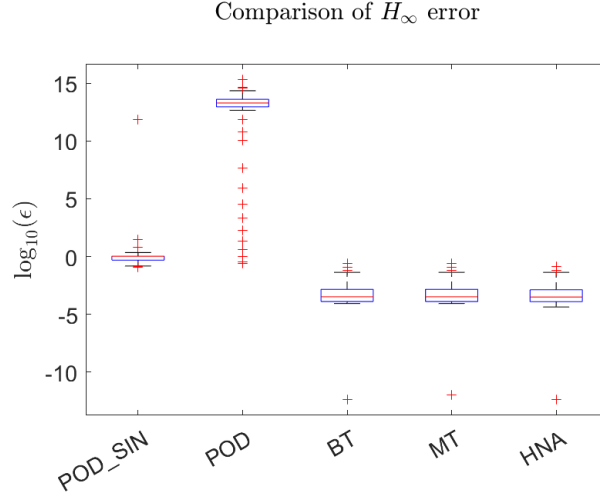


Figure 5.13.: Box Plot of H_∞ error

Where 'POD' denotes the POD ROM for $x(0, x) = 1$ and 'POD_SIN' denotes the POD ROM for $x(0, x) = \sin(\frac{2\pi}{L}x)$. The plot shows that the frequency domain error of the ROM obtained using POD with $x(0, x) = 1$ yields by far the worst results. HNA is the best choice for minimal H_∞ error. The error of HNA is slightly lower than the error of the other three methods.

5.3. Processing Time

The processing time is obtained by measuring the time it takes to build the reduced-order model. Each measurement is taken ten times to make sure that the measurements are reliable to some degree. This choice is arbitrary but was taken to keep overall computing time in check. Those measurements are depicted as box plots in the following figures.

5.3.1. Proper Orthogonal Decomposition

Figure 5.14 shows the processing time of POD. It can be observed that the time it takes to compute a POD model is quite constant for $1 \geq r \geq 100$. This implies that the implementation of the algorithm is efficient to the extent that the range of r is too small to gain information about the relation between r and the processing time. The measurements are mainly between 0.012 and 0.022 seconds.

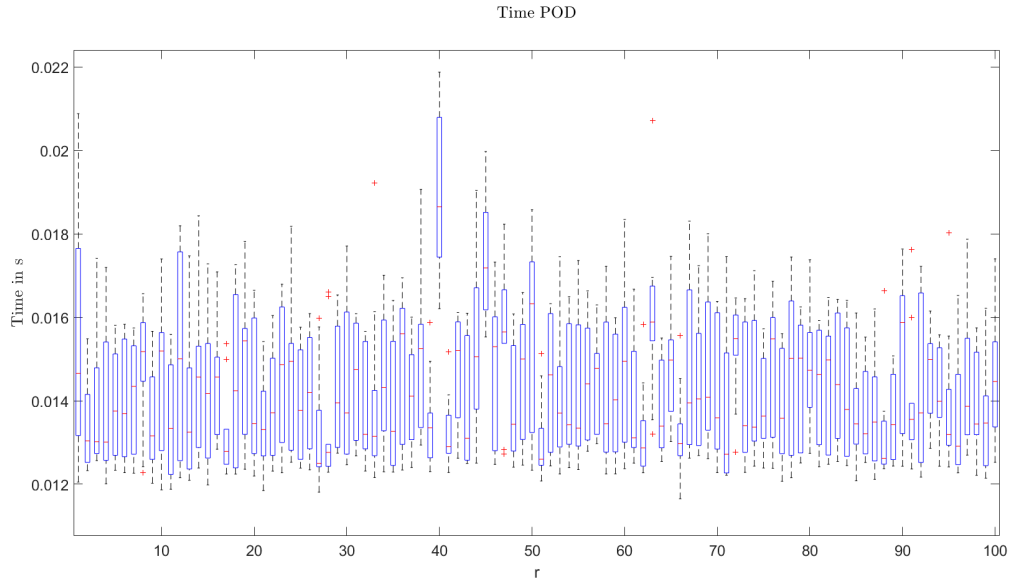


Figure 5.14.: Processing time POD

5.3.2. Modal Truncation

Figure 5.15 shows the processing time of modal truncation. It is noticeable that $r = 100$ yields the lowest time to compute. This is to be expected since, in this case, Modal truncation is equal to applying a coordinate transform to the original system. For $r \neq 100$, there is seemingly some r around fifty that offers optimal computing speed. Again this could be due to the rather small range of r . Most measurements are in a range between 3.5 and 5 milliseconds.

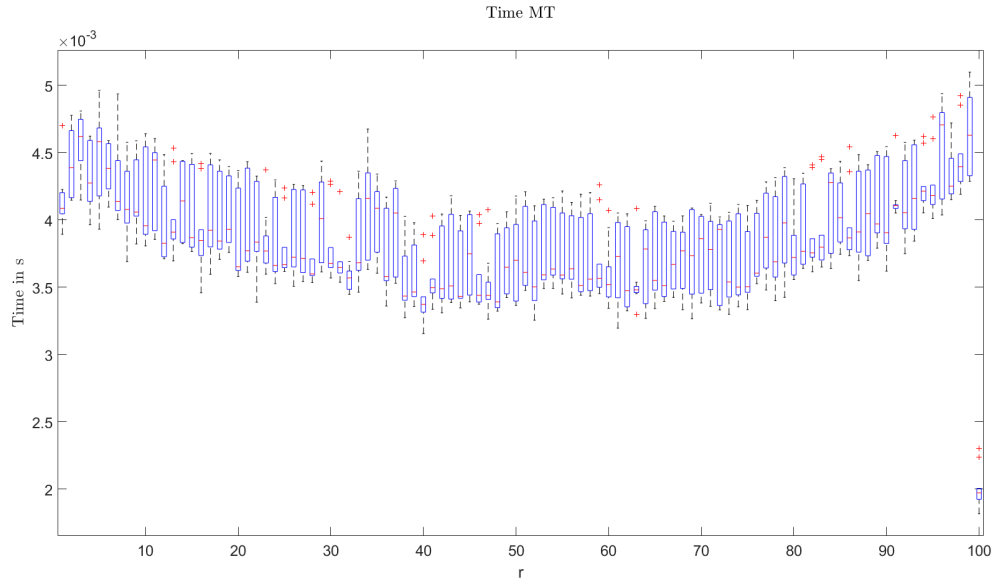


Figure 5.15.: Processing time MT

5.3.3. Balanced Truncation

Figure 5.16 displays the processing time with respect to the model order r . Again it is fairly constant where the majority of measurements are in a range between 0.03 and 0.04 seconds.

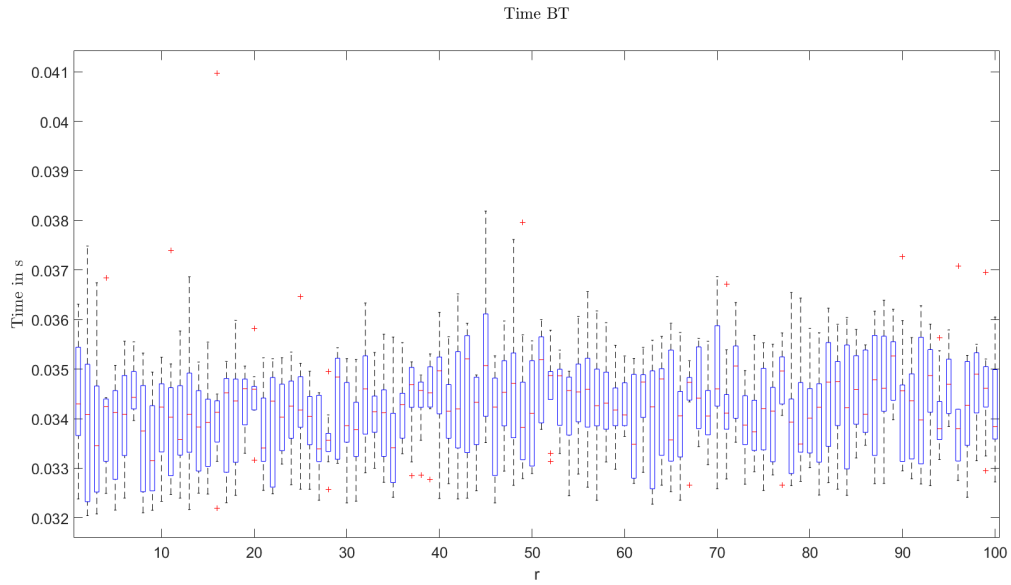


Figure 5.16.: Processing time BT

5.3.4. Hankel Norm Approximation

Figure 5.17 shows the processing time as a function of the model order. It is striking that for $r = 99$ and $r = 100$, the processing time is significantly lower than in the remaining measurements. The exact reason for this is unclear. However, it could be speculated that for $r = 100$, only a balanced realization is computed, and therefore, many algorithm steps could be skipped. Except for those two outliers, the majority of the measurements range is 0.036 to 0.043 seconds.

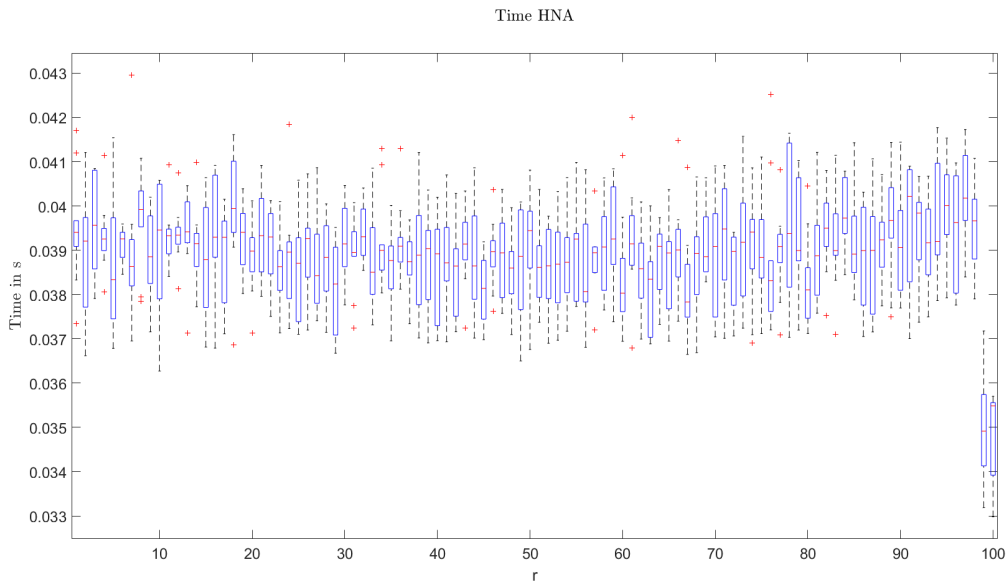


Figure 5.17.: Processing time HNA

5.3.5. Comparison of processing time

The fastest method here is modal truncation. It is roughly one order of magnitude faster than the remaining methods. Balanced truncation and Hankel norm approximation are quite similar in processing time. However, the Hankel norm approximation is slightly slower. The slowest method is the Hankel norm approximation. This is not surprising since POD uses a naive implementation. No toolbox is used. So the best method when it comes to processing speed is modal truncation.

6. Conclusion and Outlook

6.1. Conclusion

In summary, the basics were first described. First, the 1D heat equation was explained, and a naïve approach to solving it was presented. This approach had the problem that no boundary conditions could be met. For this reason, the finite element method was introduced, and then it was described how the heat equation can be discretized and solved with this method. Subsequently, various fundamentals were dealt with that were necessary for understanding the later procedures for model order reduction. These were explained in the following chapter. The orthogonal decomposition, the modal truncation, the balanced truncation, and the Hankel norm approximation were used. It is striking that the modal truncation and the balanced truncation are identical for the example system resulting from the heat equation. In the following chapter, in which the presented methods were compared in terms of $L2$ error, H_∞ error, and running time, this finding was confirmed. The errors of the modal truncation and the balanced truncation were identical. It is also noticeable that both the $L2$ error and the H_∞ error for POD depend strongly on the initial values of the system used to create the snapshot matrix. This can be explained by the fact that constant initial values, in particular, are difficult to approximate with a small number of orthogonal basis vectors, while sinusoidal initial values are straightforward to approximate. In comparison, balanced truncation and modal truncation are the best in terms of $L2$ and H_∞ errors. Hankel norm approximation is only slightly worse here. POD was by far the worst, especially if the snapshot matrix was created with constant initial values. Regarding computing time, balanced truncation and Hankel norm approximation differ only slightly. Proper orthogonal decomposition is about a factor of 2 faster here. A somewhat naïve approach was chosen to implement the POD algorithm without any particular optimization of the performance. This speaks for the simplicity of the method. Modal truncation performed best. It was about an order of magnitude faster than balanced truncation or Hankel norm approximation. Thus, modal truncation is the best method, in terms of computing time and error, for model order reduction for the system described.

6.2. Outlook

It would be worthwhile to investigate how the selected methods behave for more complex systems than the 1D heat equation. Possible systems would be 3D heat equations for inhomogeneous materials or, for example, 3D Navier-Stokes equations for the simulation of fluids. It would be interesting to choose the system so that it cannot be arbitrarily influenced from the outside and that not every state can be measured perfectly, as this has led to modal truncation and balanced truncation, giving the same results. It would also make sense to use larger initial systems for the comparisons since it has been shown that, especially in the time

measurement, only some significant statements have been made regarding the runtime as a function of the model order.

Bibliography

- [1] Gustafsson, B. “Heat Conduction”. In: *Fundamentals of Scientific Computing*. Berlin, Heidelberg: Springer Berlin Heidelberg, 2011, pp. 255–262. URL: https://doi.org/10.1007/978-3-642-19495-5_16.
- [2] Papula, L. “Gewöhnliche Differentialgleichungen”. In: *Mathematik für Ingenieure und Naturwissenschaftler Band 2: Ein Lehr- und Arbeitsbuch für das Grundstudium*. Wiesbaden: Springer Fachmedien Wiesbaden, 2015, pp. 343–541. URL: https://doi.org/10.1007/978-3-658-07790-7_4.
- [3] Gustafsson, B. “Finite Element Methods”. In: *Fundamentals of Scientific Computing*. Berlin, Heidelberg: Springer Berlin Heidelberg, 2011, pp. 173–192. URL: https://doi.org/10.1007/978-3-642-19495-5_11.
- [4] Gustafsson, B. “Polynomial Expansions”. In: *Fundamentals of Scientific Computing*. Berlin, Heidelberg: Springer Berlin Heidelberg, 2011, pp. 117–123. URL: https://doi.org/10.1007/978-3-642-19495-5_7.
- [5] Gustafsson, B. “Least Square Problems”. In: *Fundamentals of Scientific Computing*. Berlin, Heidelberg: Springer Berlin Heidelberg, 2011, pp. 125–133. URL: https://doi.org/10.1007/978-3-642-19495-5_8.
- [6] Gustafsson, B. “Elementary Functions”. In: *Fundamentals of Scientific Computing*. Berlin, Heidelberg: Springer Berlin Heidelberg, 2011, pp. 77–99. URL: https://doi.org/10.1007/978-3-642-19495-5_5.
- [7] Brunton, S. L./ Kutz, J. N. “Singular Value Decomposition (SVD)”. In: *Data-Driven Science and Engineering: Machine Learning, Dynamical Systems, and Control*. Cambridge University Press, 2019, pp. 3–46.
- [8] Brunton, S. L./ Kutz, J. N. “Fourier and Wavelet Transforms”. In: *Data-Driven Science and Engineering: Machine Learning, Dynamical Systems, and Control*. Cambridge University Press, 2019, pp. 47–83.
- [9] Szabo, F. E. “U”. In: *The Linear Algebra Survival Guide*. Ed. by Szabo, F. E. Boston: Academic Press, 2015, pp. 385–392. URL: <https://www.sciencedirect.com/science/article/pii/B978012409520550028X>.

- [10] Naoko, S. *Geometric Interpretation of the Correlation between Two Variables*. 2018. URL: <https://medium.com/@ns2586/geometric-interpretation-of-the-correlation-between-two-variables-4011fb3ea18e> (visited on 03/01/2023).
- [11] Oliver, K. *Math 19b: Linear Algebra with Probability*. 2011. URL: https://people.math.harvard.edu/%5C~knill/teaching/math19b_2011/handouts/lecture12.pdf (visited on 03/01/2023).
- [12] Victor, L. *IAML: Dimensionality Reduc6on*. 2011. URL: <https://www.inf.ed.ac.uk/teaching/courses/iaml/2011/slides/pca.pdf> (visited on 03/01/2023).
- [13] Douglas, B. “The Fundamentals of Control Theory”. In: Academia, 2019, pp. 8–15.
- [14] Douglas, B. “The Fundamentals of Control Theory”. In: Academia, 2019, pp. 42–47.
- [15] Benner, P. et al. “1 Model order reduction: basic concepts and notation”. In: *Volume 1 System- and Data-Driven Methods and Algorithms*. Ed. by Benner, P. et al. Berlin, Boston: De Gruyter, 2021, pp. 1–14. URL: <https://doi.org/10.1515/9783110498967-001>.
- [16] Brunton, S. L./ Kutz, J. N. “Linear time-invariant systems”. In: *Data-Driven Science and Engineering: Machine Learning, Dynamical Systems, and Control*. Cambridge University Press, 2019, p. 334.
- [17] Douglas, B. “The Fundamentals of Control Theory”. In: Academia, 2019, pp. 48–63.
- [18] Abell, M. L./ Braselton, J. P. “Chapter 8 - Introduction to the Laplace Transform”. In: *Introductory Differential Equations (Fifth Edition)*. Ed. by Abell, M. L./ Braselton, J. P. Fifth Edition. Academic Press, 2018, pp. 399–460. URL: <https://www.sciencedirect.com/science/article/pii/B9780128149485000082>.
- [19] Brunton, S. L./ Kutz, J. N. “CONTROLLABILITY AND OBSERVABILITY”. In: *Data-Driven Science and Engineering: Machine Learning, Dynamical Systems, and Control*. Cambridge University Press, 2019, pp. 335–341.
- [20] *Volume 1 System- and Data-Driven Methods and Algorithms*. Berlin, Boston: De Gruyter, 2021. URL: <https://doi.org/10.1515/9783110498967>.

- [21] Gustafsson, B. “Polynomial Expansions”. In: *Fundamentals of Scientific Computing*. Berlin, Heidelberg: Springer Berlin Heidelberg, 2011, pp. 117–123. URL: https://doi.org/10.1007/978-3-642-19495-5_7.
- [22] Gustafsson, B. “Numerical Methods for Differential Equations”. In: *Fundamentals of Scientific Computing*. Berlin, Heidelberg: Springer Berlin Heidelberg, 2011, pp. 137–144. URL: https://doi.org/10.1007/978-3-642-19495-5_9.
- [23] Brunton, S. L./ Kutz, J. N. “Reduced Order Models (ROMs)”. In: *Data-Driven Science and Engineering: Machine Learning, Dynamical Systems, and Control*. Cambridge University Press, 2019, pp. 375–402.
- [24] Brunton, S. L./ Kutz, J. N. “Discrete Fourier transform (DFT) and fast Fourier transform (FFT)”. In: *Data-Driven Science and Engineering: Machine Learning, Dynamical Systems, and Control*. Cambridge University Press, 2019, pp. 71–73.
- [25] Ruppert, F. *Differentiation mit Matrizen*. matheplanet.com. URL:<https://www.matheplanet.com> (version: 2014-03-13). eprint: <https://www.matheplanet.com/matheplanet/nuke/html/viewtopic.php?rd2\&topic=128338\&start=0\#p937673>. URL: <https://www.matheplanet.com/matheplanet/nuke/html/viewtopic.php?rd2%5C&topic=128338%5C&start=0%5C#p937673>.
- [26] Kloos, J. *When is matrix multiplication commutative?* Mathematics Stack Exchange. URL:<https://math.stackexchange.com/q/170371> (version: 2014-03-13). eprint: <https://math.stackexchange.com/q/170371>. URL: <https://math.stackexchange.com/q/170371>.
- [27] Sapir, D. M. V. *Symmetric, diagonal, triangular matrices*. Linear Algebra Web-Notes. URL: <https://math.vanderbilt.edu/sapirmv/msapir/jan22.html#:~:text=following%20result%20holds-,Theorem.,B%20then%20AB%20is%20symmetric..>
- [28] Brunton, S. L./ Kutz, J. N. “BALANCED MODELS FOR CONTROL”. In: *Data-Driven Science and Engineering: Machine Learning, Dynamical Systems, and Control*. Cambridge University Press, 2019, pp. 376–388.
- [29] Vuillemin, P./ Maillard, A./ Poussot-Vassal, C. *Optimal Modal Truncation*. 2020. arXiv: 2009.11540 [math.OC].
- [30] Peter Benner, L. F. *Model Reduction for Dynamical Systems — Lecture 4* —. 2015. URL: <https://www.mpi-magdeburg.mpg.de/2925234/lecture4.pdf> (visited on 04/03/2023).

- [31] Singh, N. “Reduction of linear dynamic systems using hankel norm approximation”. In: *Control and Intelligent Systems* 41 (01/2013).
- [32] GLOVER, K. “All optimal Hankel-norm approximations of linear multivariable systems and their L , ∞ -error bounds†”. In: *International Journal of Control* 39.6 (1984), pp. 1115–1193. eprint: <https://doi.org/10.1080/00207178408933239>. URL: <https://doi.org/10.1080/00207178408933239>.
- [33] Sandberg, H. “Introduction to Model Order Reduction”. In: (07/2019), pp. 45–48. URL: <http://www.diva-portal.org/smash/get/diva2:1338145/FULLTEXT01.pdf> (visited on 04/15/2023).
- [34] Zhang, X. *The properties and application of symmetric matrice*. 09/2021. URL: <https://towardsdatascience.com/the-properties-and-application-of-symmetric-matrice-1dc3f183de5a> (visited on 04/21/2023).
- [35] (<https://math.stackexchange.com/users/57021/yiorgos-s-smylis>), Y. S. S. *Integral of matrix exponential*. Mathematics Stack Exchange. URL: <https://math.stackexchange.com/q/658289> (version: 2020-10-28). eprint: <https://math.stackexchange.com/q/658289>. URL: <https://math.stackexchange.com/q/658289>.
- [36] Benner, P./ Werner, S. W. R. *Morlab*. URL: <https://www.mpi-magdeburg.mpg.de/projects/morlab> (visited on 02/27/2023).
- [37] Systems, P. D. *MOR toolbox*. URL: <https://mordigitalsystems.fr/en/products.html> (visited on 02/27/2023).
- [38] Schuster, E. *System Identification and Robust Control*. 2020. URL: https://www.lehigh.edu/~eus204/teaching/ME450_SIRC/lectures/lecture07.pdf (visited on 04/23/2023).
- [39] D’Erchie, M. e. a. “Analysis Eins”. In: *Mathe für Nicht-Freaks*. Serlo Education e. V., 2017, pp. 111–113. URL: https://mathe-builds.serlo.org/analysis1_final/analysis1_final.pdf.
- [40] Alexandre M. Bayen, T. S. “An Introduction to MATLAB® Programming and Numerical Methods for Engineers”. In: Science Direct, 2015, pp. 211–214. URL: <https://www.sciencedirect.com/book/9780124202283/an-introduction-to-matlab-programming-and-numerical-methods-for-engineers>.

A. Appendix

A.1. Deriving matrices for FEM using piecewise linear functions

The so called triangle function is defined as follows:

$$\phi_j(x) = \begin{cases} (x - x_{j-1})/\Delta x, & x_{j-1} \leq x < x_j \\ (x_{j+1} - x)/\Delta x, & x_j \leq x < x_{j+1} \\ 0, & \text{otherwise} \end{cases} \quad (\text{A.1})$$

[4]

The following integrals have to be evaluated:

$$\int_{\chi} \phi_j \phi_k dx \quad \forall \phi_k \in \phi \quad (\text{A.2})$$

$$- \int_{\chi} \frac{d\phi_j}{dx} \frac{d\phi_k}{dx} dx \quad \forall \phi_k \in \phi \quad (\text{A.3})$$

With $\chi \subset \mathbb{R}$. Note that the product of two functions ϕ_j and ϕ_k and their derivatives is only under two conditions not zero:

1. $k = j$

Considering this case the integral A.2 becomes:

$$\int_{x_{j-1}}^{x_j} \phi_j^2 dx + \int_{x_j}^{x_{j+1}} \phi_j^2 dx \quad (\text{A.4})$$

Because of symmetry only one of the above integrals have to computed:

$$2 \int_{x_{j-1}}^{x_j} \phi_j^2 dx \quad (\text{A.5})$$

$$= \frac{2}{\Delta x^2} \int_{x_{j-1}}^{x_j} (x - x_{j-1})^2 dx \quad (\text{A.6})$$

$$\frac{2}{3\Delta x^2} [(x - x_{j-1})^3]_{x_{j-1}}^{x_j} = \frac{2}{3\Delta x^2} \Delta x^3 = \frac{2}{3} \Delta x \quad (\text{A.7})$$

Integral A.3 for $i = j$ taking symmetry into account becomes:

$$- \int_{x_{j-1}}^{x_{j+1}} \left(\frac{d\phi_j}{dx} \right)^2 dx = - \frac{1}{\Delta x^2} \int_{x_{j-1}}^{x_{j+1}} 1 dx \quad (\text{A.8})$$

$$= - \frac{1}{\Delta x^2} [x]_{x_{j-1}}^{x_{j+1}} = - \frac{2}{\Delta x} \quad (\text{A.9})$$

2. $|j - k| = 1$ A.2 becomes:

$$\frac{1}{\Delta x^2} \int_{x_j}^{x_{j+1}} (x - x_j)(x_{j+1} - x) dx \quad (\text{A.10})$$

$$= \left[\frac{1}{2} x^2 x_{j+1} - \frac{1}{3} x^3 - x x_{j+1} x_j + \frac{1}{2} x^2 x_j \right]_{x_j}^{x_{j+1}} = \frac{1}{6\Delta x^2} \Delta x^3 = \frac{1}{6} \Delta x \quad (\text{A.11})$$

Finally A.3 has to be evaluated for this condition:

$$- \int_{x_j}^{x_{j+1}} \frac{d\phi_j}{dx} \frac{d\phi_{j+1}}{dx} dx = \frac{1}{\Delta x^2} \int_{x_j}^{x_{j+1}} 1 dx = \frac{1}{\Delta x^2} [x]_{x_j}^{x_{j+1}} = \frac{1}{\Delta x} \quad (\text{A.12})$$

A.2. Proof that matrix **M** is invertible

Let M_n be a matrix with $M_n \in \mathbb{R}^{n \times n}$ given by:

$$m_{ij} = \begin{cases} a, & k = j \\ b, & |k - j| = 1 \\ 0, & otherwise \end{cases} \quad (\text{A.13})$$

It's determinant is given by the Laplace expansion:

$$\det(M_n) = \sum_{j=1}^n (-1)^{i+j} a_{ij} N_{ij} \quad \forall i \quad (\text{A.14})$$

N_{ij} is the determinant of the matrix M' that is obtained by removing the i^{th} row and j^{th} column of M_n . This expression can be simplified using the definition of m_{ij} :

$$\det(M_n) = aN_{11} - bN_{12} \quad (\text{A.15})$$

N_{11} is equivalent to $\det(M_{n-1})$, since the indices of rows and columns of M' are in consecutive order and M' is a $n - 1 \times n - 1$ matrix :

$$N_{11} = \det(M') \quad (\text{A.16})$$

$$M' = \begin{bmatrix} m_{22} & \dots & m_{2n} \\ \vdots & \ddots & \vdots \\ m_{n2} & \dots & m_{nn} \end{bmatrix} \quad (\text{A.17})$$

N_{12} can be obtained by calculating the determinant of M' using the Laplace expansion:

$$M' = \begin{bmatrix} m_{21} & m_{23} & \dots & m_{2n} \\ \vdots & \vdots & \ddots & \vdots \\ m_{n1} & m_{n3} & \dots & m_{nn} \end{bmatrix} \quad (\text{A.18})$$

$$\det(M') = m_{21} \cdot \det(M'') \quad (\text{A.19})$$

$$M'' = \begin{bmatrix} m_{33} & \dots & m_{3n} \\ \vdots & \ddots & \vdots \\ m_{n3} & \dots & m_{nn} \end{bmatrix} \quad (\text{A.20})$$

In A.19 only the stated term has to be evaluated since all entries of the first column of the second sub matrix are zero. Therefore the determinant is zero. The row and column indices of M'' are in consecutive order and it is a $n-2 \times n-2$ matrix. Therefore M'' is equivalent to M_{n-2} . A.15 becomes:

$$\det(M_n) = a \cdot \det(M_{n-1}) - b^2 \cdot \det(M_{n-2}) \quad (\text{A.21})$$

Furthermore this implies $\det(M_0) = 1$:

$$\det(M_2) = a^2 - b^2 = a \cdot \det(M_1) - b^2 \cdot 1 \quad (\text{A.22})$$

$$\Rightarrow \det(M_0) = 1 \quad (\text{A.23})$$

Using the definition of 2.34 and 2.2.1 this can be seen as the following sequence:

$$a_0 = 1, \quad a_1 = \frac{2\Delta x}{3} \quad (\text{A.24})$$

$$a_{n+1} = \frac{2\Delta x}{3} \cdot a_n - \frac{\Delta x^2}{36} \cdot a_{n-1} \quad (\text{A.25})$$

As described here [39] a recursive sequence converges if it is monotone and has a limit. A proof by induction shows that this sequence is monotone for $n \geq 1$.

Base case:

$$a_2 = \left(\frac{2\Delta x}{3}\right)^2 - \frac{\Delta x^2}{36} = \Delta x^2 \left(\frac{4}{9} - \frac{1}{36}\right) < \frac{2\Delta x}{3} = a_1 \quad (\text{A.26})$$

Induction step: Assuming that $a_k < a_{k-1}$ holds, $a_{k+1} < a_k$ also holds:

$$a_{k+1} = \frac{2\Delta x}{3} \cdot a_k - \frac{\Delta x^2}{36} \cdot a_{k-1} < \frac{2\Delta x}{3} \cdot a_{k-1} - \frac{\Delta x^2}{36} \cdot a_{k-2} = a_k \quad (\text{A.27})$$

The limit of this sequence is as follow:

$$\alpha = \lim_{n \rightarrow \infty} a_{n+1} = \lim_{n \rightarrow \infty} \Delta x \cdot \frac{2}{3} \cdot \lim_{n \rightarrow \infty} a_n - \lim_{n \rightarrow \infty} \Delta x^2 \cdot \frac{1}{36} \cdot \lim_{n \rightarrow \infty} a_{n-1} = 0 \cdot \alpha - 0 \cdot \alpha = 0 \quad (\text{A.28})$$

Since this series is monotone and converges to zero as n goes to infinity, there is no $n \in \mathbb{N}$ for which $a_n = 0$. Therefore the determinant of the matrix M defined in 2.34 is not zero and M is invertible.

A.3. Equivalence of picewise linear polynomials and linear interpolation

A picewise linear polynomial in the form of:

$$u(x, t) = \sum_{j=1}^N c_j(t) \phi_j(x) \quad (\text{A.29})$$

With ϕ_j being defined as A.1 and $c_j : \mathbb{R} \rightarrow \mathbb{R}$ is equivalent to linear interpolation with respect to x :

$$\hat{u}(x, t) = u_j + \frac{(u_{j+1} - u_j)(x - x_j)}{x_{j+1} - x_j} \quad (\text{A.30})$$

for $x_j < x < x_{j+1}$ [40]. This can be shown by evaluating $u(x, t)$ between two neighbouring ϕ and $x_j < x < x_{j+1}$:

$$u(x, t) = \phi_j(x) c_j(t) + \phi_{j+1}(x) c_{j+1}(t) \quad (\text{A.31})$$

$$= \frac{x_{j+1} - x}{\Delta x} c_j(t) + \frac{x - x_j}{\Delta x} c_{j+1}(t) \quad (\text{A.32})$$

$$= \frac{x_{j+1} - x}{\Delta x} u_j + \frac{x - x_j}{\Delta x} u_{j+1} \quad (\text{A.33})$$

$$= \frac{(x_{j+1} u_j - x u_j) + (x u_{j+1} - x_j u_{j+1})}{\Delta x} \quad (\text{A.34})$$

$$= \frac{(u_{j+1} - u_j)x + x_{j+1} u_j - x_j u_{j+1}}{\Delta x} \quad (\text{A.35})$$

$$= \frac{(u_{j+1} - u_j)x + x_j u_j + \Delta x u_j - x_j u_{j+1}}{\Delta x} \quad (\text{A.36})$$

$$= u_j + \frac{(u_{j+1} - u_j)x - x_j(u_{j+1} - u_j)}{\Delta x} \quad (\text{A.37})$$

$$= u_j + \frac{(u_{j+1} - u_j)(x - x_j)}{x_{j+1} - x_j} \quad (\text{A.38})$$